T-Cell-Mediated Killing in Glioblastoma Organoids induced by Adenoviral Delivery of the CIITA Transgene

Ilaria Salvato[1,2,3,*], Eliane Klein[1,3,*], Aurélie Poli[4], Mahsa Rezaeipour[1], Luca Ermini[1], Bakhtiyor Nosirov[1,5], Anuja Lipsa[1], Anais Oudin[1], Virginie Baus[1], Gian Mario Dore[2], Antonio Cosma[6], Anna Golebiewska[1], Antonio Marchini[2,7,8,§], Simone P. Niclou[1,3,§]

[1]NORLUX Neuro-Oncology Laboratory, Department of Cancer Research, Luxembourg Institute of Health (LIH), Luxembourg;

[2]Laboratory of Oncolytic Virus Immuno-Therapeutics (LOVIT), Department of Cancer Research, Luxembourg Institute of Health (LIH), Luxembourg;

[3]Department of Life Sciences and Medicine, Faculty of Science, Technology and Medicine (FSTM), University of Luxembourg, Luxembourg;

[4]Neuro-Immunology Group, Department of Cancer Research, Luxembourg Institute of Health (LIH), Luxembourg;

[5]Multiomics Data Science Research Group, Department of Cancer Research, Luxembourg Institute of Health (LIH), Luxembourg;

[6]National Cytometry Platform, Translational Medicine Operation Hub, Luxembourg Institute of Health, Esch-sur-Alzette, Luxembourg;

[7]Laboratory of Oncolytic Virus Immuno-Therapeutics, German Cancer Research Center, Heidelberg, Germany.

[8]Current address: European Commission, Joint Research Centre (JRC), Geel, Belgium;

* Equal contribution

§ Co-senior authors and corresponding authors

ABSTRACT

The immunosuppressive nature of the tumor microenvironment poses a significant challenge to effective immunotherapies against glioblastoma (GB). Boosting the immune response is critical for a successful therapy. Here, we adopted a cancer gene therapy approach to induce T-cell mediated killing of the tumor through increased activation of the immune system. Patient-based 3D GB models were infected with a replication-deficient adenovirus (AdV) armed with the Class II Major Histocompatibility Complex (MHC-II) Transactivator *CIITA* gene (Ad-CIITA). Successful induction of surface MHC-II was achieved in infected GB cell lines and primary human GB organoids. Infection with an AdV carrying a mutant form of *CIITA* with a single amino acid substitution resulted in cytoplasmic accumulation of CIITA without subsequent MHC-II expression. Co-culture of infected tumor cells with either PBMCs or isolated T-cells led to dramatic breakdown of GB organoids. Intriguingly, both wild-type and mutant Ad-CIITA but not unarmed AdV, triggered immune-mediated tumor cell death in the co-culture system, suggesting an at least partially MHC-II-

independent process. We further show that the observed cancer cell killing requires the presence of either $CD8^+$ or $CD4^+$ T-cells and the direct contact between GB and immune cells. We did not however detect evidence of activation of canonical T-cell mediated cell death pathways. While the precise mechanism remains to be determined, these findings highlight the potential of AdV-mediated *CIITA* delivery to enhance T-cell-mediated immunity against GB.

KEYWORDS

Glioblastoma/Adenovirus/Gene therapy/MHC-II/T-cells/Tumor Organoids

INTRODUCTION

Malignant brain tumors including glioblastoma (GB) remain a major clinical and scientific challenge. The immunosuppressive tumor microenvironment (TME) as well as systemic immunosuppression pose challenges to current immunotherapies. GBs recruit immunosuppressive cells like tumor-associated microglia and macrophages (TAMs) and regulatory T-cells (Tregs), while only a limited number of T-cells are present, often showing signs of exhaustion[1-3]. GB tumors may also downregulate the expression of major histocompatibility complex (MHC) molecules that play a central role in presenting cancer-derived antigens to the immune system[4].

Despite promising results in preclinical studies, immunotherapies, whether tested individually or in combination with standard care, have so far failed to translate in clinically meaningful outcomes for GB patients [5]. This discrepancy can be largely attributed to oversimplified preclinical models that do not recapitulate the complex biology of GBs. Replication-deficient adenoviruses (AdVs) have demonstrated safety and tolerability in the treatment of various cancer types, including GB. Current GB treatments using AdVs focus on the delivery of herpes simplex virus (HSV) thymidine kinase (TK), p53, interleukin (IL)-12, interferon (IFN)-β, and a chimeric death receptor (VB-111)[5].

A promising approach is to arm non-lytic AdV vectors with transgenes to boost anti-GB immunity. Class II Major Histocompatibility Complex Transactivator (CIITA) is the master regulator of MHC class II (MHC-II) molecules, typically expressed in professional antigen presenting cells (APCs)[6]. Upon expression and translocation to the nucleus, CIITA interacts with the constitutively-expressed factors of the enhanceosome complex and activates the transcription of cell surface "classical" human leukocyte antigen (HLA)-DR, HLA-DP and HLA-DQ, which present antigens to $CD4^+$ T-cells, as well as HLA-DM, HLA-DO and invariant chain (Ii), involved in intracellular antigen processing[7].

Previous work on carcinoma cell lines[8-10], and more recently on murine glioma cells[11], found that ectopic stable expression of CIITA transforms tumor cells into MHC-II-positive cells with enhanced antigen processing and presentation capabilities. Remarkably, CD80 and CD86 costimulatory molecules, essential alongside MHC-II expression, were discovered to be dispensable for T-cell activation[8, 12, 13]. In these models, CIITA-transfected/infected MHC-II-positive cells were found to prime and activate $CD4^+$ T-cells, resulting in tumor rejection or growth retardation in mice with subcutaneous tumors[10-13]. However, direct antigen presentation and antigen-based T-cell activation have not been reported. A recent study indicated limited pro-immunogenic potential of CIITA in GB tumors[14].

Here, we engineered a replication-deficient AdV with *CIITA* to infect patient-derived GB organoids and promote antitumor immunity. We established an advanced human GB co-culture system, based on primary organoids co-cultured with human immune cells, to assess the functional impact of the gene therapy approach in a complex model. We find that AdV-mediated delivery of *CIITA* induces cancer cell death in the presence of immune cells. While the exact mechanism remains to be elucidated, our data suggest that the effect is at least partially independent of MHC-II expression.

RESULTS

MHC-II expression in GB is limited to non-neoplastic cells of the tumor microenvironment.

To assess the diversity of MHC-II molecules in GB, we examined gene expression profiles at bulk and single-cell level in patient tumors and preclinical models. At bulk RNA level, expression of *CIITA* and genes coding for MHC-II antigen presenting molecules (*HLA-DQA1*, *HLA-DQB1*, *HLA-DRA, HLA-DRB1, HLA-DRB5)* was higher in GBs than in normal brain tissue (**Fig.1A**). However, analysis of single-cell RNA-sequencing (RNA-seq) of GB patient tumors revealed that tumor cells do not express *CIITA* nor genes encoding for MHC-II antigen processing (*CD74*, *HLA-DMA*, *HLA-DOA*) and presentation (*HLA-DQA1*, *HLA-DQB1*, *HLA-DRA, HLA-DRB1, HLA-DRB5)* (**Fig.1B**). High expression of these genes was detected in immune cells of the TME, explaining the high transcript levels observed by bulk RNA-seq. The highest MHC-II expression was detected in well-known APCs, including dendritic cells, macrophages, microglia, and B cells (**Fig.1B**). Limited cancer cell expression of MHC-II genes was confirmed in a cohort of 28 GB patient-derived orthotopic xenografts (PDOXs), where bulk RNA-seq profiles showed low expression of human genes involved in MHC-II antigen processing and presentation and moderately high levels of enhanceosome-associated genes (**Fig.1C**). Except for U87 cell line, similar expression profiles were seen in human GB cell lines, including adherent and 3D sphere cultures of GB stem-like cells (GSCs) (**Supplementary Fig.1A**). Interestingly, the genes associated with the MHC-II enhanceosome complex (*CREB1*, *NFYA*, *NFYB*, *NFYC*, *RFX5*, *RFXANK*, and *RFXAP)* showed sustained expression throughout patient tumors, PDOX and cell lines (**Supplementary Fig.1A**), suggesting that GB cells have the capacity to express MHC-II upon activation of the MHC-II master regulator CIITA. Moreover, most of the preclinical models exhibited transcriptional expression of the Coxsackie and Adenovirus Receptor (*CXADR*), the specific receptor for AdV serotype 5, as well as the integrin αvβ5 necessary for AdV infection (*ITGAV* and *ITGB5*)[15] (**Fig.1C, Supplementary Fig.1A**). This observation implies that GB tumor cells are likely to be susceptible to AdV infection, highlighting the suitability of non-lytic AdVs for targeting GB.

Next, we assessed the presence of MHC-II proteins at the cell surface of GB cells by flow cytometry. The majority of GB cells showed no MHC-II protein at the cell surface under regular culture conditions (**Fig.1D, Supplementary Fig.1B**). Out of 10 GB cell lines analyzed, only U87 and BG5 cells showed some positive cells (17.9% and 9.6% respectively). Interestingly, IFN-γ cytokine stimulus did not activate MHC-II expression in GB cells, except for U87, BG5, and T16NS (**Fig.1D**).

In summary, we confirmed that MHC-II molecules are largely absent from GB tumor cells but are expressed in tumor-associated APCs. Based on the presence of transcripts of the MHC-II enhanceosome complex, ectopic expression of CIITA appears as a valid strategy to deliver MHC-II

molecules at the cell membrane. Moreover, the expression of the necessary AdV receptor and cell adhesion molecules confers infectivity to GB cells to serotype 5 AdVs.

Human GB stem-like cells infected with Ad-CIITA express CIITA and present MHC-II molecules at the cell surface.

To convert MHC-II-negative GB tumor cells into APC-like cells, we generated a replication-deficient AdV carrying the wild-type *CIITA* gene (Ad-CIITA) (**Fig.2A**) or a mutated *CIITA* transgene (Ad-CIITA mutant). The mutant CIITA carried a novel missense point mutation (guanine-to-adenosine) (**Supplementary Fig.2A**) leading to a single amino acid substitution (glycine (G) to arginine (A)) at position 1088 (**Supplementary Fig.2B**). Serendipitously generated by us, we found that this mutation impaired the translocation of CIITA to the cell nucleus (**Supplementary Fig.2C**). AdV vectors without transgene (Ad-null) or with the green fluorescent protein (GFP)-encoding transgene (Ad-GFP) were used as controls (**Fig.2A**).

Optimal viral infection and appropriate CIITA and MHC-II expression were determined in the mouse GB cell line GL261 (**Supplementary Fig.2D-E**). In human GSC lines (P3NS and T16NS), CIITA mRNA (**Fig.2B**) and protein (**Fig.2C**) were detected at 72 hours post-infection with both Ad-CIITA and Ad-CIITA mutant. Only wild-type CIITA induced HLA-DRα mRNA and protein expression (**Fig.2B-C**), the latter was confirmed at the cell membrane (**Fig.2D**). In summary, we successfully generated an Ad-CIITA vector that led to surface MHC-II expression in human GB cells. Ad-CIITA mutant vector did not induce MHC-II expression allowing to distinguish between nuclear and non-nuclear CIITA effects.

Infection with Ad-CIITA induces MHC-II expression in human primary GB organoids.

We next determined the efficacy of Ad-CIITA in primary GB organoids from different patients (P3, T16 and T188), representing tumors with classical genetic and epigenetic features (**Table S1**). In P3 organoids, a viral multiplicity of infection (MOI) between 25 and 100 led to strong ectopic expression of CIITA and HLA-DRα at 72-post-infection (**Fig.3A**), whithout a major effect on tissue structure (**Fig.3B**). Again, only Ad-CIITA-infected cells showed MHC-II expression (**Fig.3B**, lower panel), also confirmed by flow cytometry (**Fig.3C**). MHC-I (HLA-A/B/C) expression remained largely unaltered, while CD80 or CD86 co-stimulatory molecules were undetectable at baseline or upon infection (**Supplementary Fig.3A**).

To evaluate potential adverse effects of AdV, dsRed-expressing P3 organoids were infected at increasing MOIs, and dsRed fluorescence intensity was monitored in real-time. As expected[16], viral infection caused a small dose-dependent reduction in organoid growth rate, independent of the transgene, but did not show signs of cell death (**Fig.3D**). H&E-stained sections confirmed this observation (**Fig.3B**). Similar results were seen in T16 organoids, while T188 organoids were unaffected by viral infection (**Supplementary Fig.3B**). In conclusion, AdVs effectively infect primary GB organoids with minimal impact on tumor growth. Robust MHC-II expression is obtained with Ad-CIITA, but not with Ad-CIITA mutant or Ad-null vectors.

159 **Ad-CIITA-triggered immune-mediated tumor cell death is mediated by CD3$^+$ T-cells but is largely**
160 **independent of MHC-II expression.**

161 To evaluate the potential of MHC-II-expressing human GB to elicit adaptive immune responses, we
162 established a protocol involving the co-culture of virally-infected primary GB organoids with
163 allogenic immune cells, from healthy donors or from partially HLA-matched donors (**Fig.4A**). The
164 purity of PBMCs and isolated cell types were assessed by flow cytometry before co-culture
165 (**Supplementary Fig.4A, Table S2**).

166 Based on previous tumor-immune cell co-culture studies[17], we first used immune cells from healthy
167 human donors. In co-culture conditions without immune cells, P3 GB organoids retained their
168 structure, their proliferation being slightly affected by viral infection (**Fig.4B**), in line with the
169 experiments shown in **Fig.3D**. Upon addition of allogenic PBMCs, we observed a pronounced
170 organoid disruption and tumor cell killing in Ad-CIITA-infected organoids (86,5%±10,2), contrasting
171 with a lower effect in Ad-null-infected organoids (42,2%±7,3) (**Fig.4B, Video S1**). Percentages
172 represent the reduction in dsRed signal compared to non-infected controls at the co-culture end-
173 point. Interestingly, the Ad-CIITA mutant also led to robust tumor cell killing in the presence of
174 PBMCs (78,3%±21,7) (**Fig.4B, Video S1**), despite the lack of MHC-II expression (**Fig.3C**). Similar
175 results were seen in T16 and T188 organoids, where pronounced tumor cell death was induced by
176 Ad-CIITA and again, though to a lesser extent, by Ad-CIITA mutant (**Supplementary Fig.4B**). These
177 data suggest that CIITA expression potentiates the immunogenicity of GB organoids for alloreactive
178 PMBCs, potentially mediated by a cumulative effect of MHC-II-dependent and independent
179 mechanisms.

180 We next sought to determine whether CD3+ T-cells were involved in the observed killing
181 phenotype. Similar to PBMCs, purified CD3$^+$ T-cells alone efficiently induced tumor cell killing in P3
182 organoids infected with Ad-CIITA (76,4%±21,9) or Ad-CIITA mutant (75,1%±29,4), suggesting a
183 primary T-cells involvement (**Fig.4C vs Fig.4B**). Immune-mediated tumor cell death was further
184 confirmed by flow cytometry (**Fig.4D**). To assess the specificity of Ad-CIITA induced T-cell killing, we
185 performed co-culture experiments with purified CD4$^+$ and CD8$^+$ T-cells, which rely on MHC-II and
186 MHC-I molecules, respectively. Efficient tumor cell killing was maintained with either CD4$^+$ (Ad-
187 CIITA: 75,6%±16,8) or CD8$^+$ T-cells (Ad-CIITA: 67,5%±28,8) (**Fig.4C**). Similar results were obtained
188 with T16 and T188 organoids (**Supplementary Fig.4C**), reinforcing the involvement of a MHC-II-
189 independent mechanism in GB cell killing. Nevertheless, we next aimed to exclude a purely
190 alloreactive T-cell reaction, by applying effector cells sharing a partial match at HLA alleles with the
191 target GB organoids. Unfortunately, autologous PBMCs from the tumor patient were not available.
192 Specifically, PBMCs were chosen to match the HLA typing of the donor GB tumors at least at one
193 allele of each MHC-I (*HLA-A*, *HLA-B*, *HLA-C*) and each MHC-II (*HLA-DRB1/3/4/5*, *HLA-DQA1*, *HLA-*
194 *DQB1*, *HLA-DPA1*, *HLA-DPB1*) locus. The matching degree varied depending on the donor, as
195 presented in **Table S3**. The Ad-CIITA-mediated killing phenotype was retained in the P3 co-culture
196 model (**Fig.4E**) and confirmed in T16 tumors (**Supplementary Fig.4D**). Although the cytotoxic
197 activity of HLA-matched PBMCs and isolated CD3$^+$ cells was reduced compared to allogenic PBMCs
198 (**Fig.4C vs Fig.4E**), these data confirmed that the main killing activity observed could not be
199 attributed to an alloreactive immune reaction linked to mismatching MHC molecules.

200 In summary, our findings show that both Ad-CIITA and Ad-CIITA mutant enhance the
201 immunogenicity of GB for allogenic T-cells, facilitating efficient tumor cell killing in the presence of
202 either CD4+ or CD8+ T-cells. These data suggest that CIITA activates a T-cell-mediated immune
203 response that is at least partially independent of MHC-II antigen presentation.

204

205 **Immune-mediated tumor cell killing of GB organoids requires CIITA expression and cell-to-cell**
206 **contact with T-cells, but no antigen presentation.**

207 To address the functionality of MHC-II molecules induced by Ad-CIITA, we used a proliferation assay
208 of T-cells from OT-II mice, specifically reacting to ovalbumin peptides 323-339 (OVA323-339)
209 (**Fig.5A**). In contrast to the positive control, $CD3^+$ T-cells co-cultured with Ad-CIITA-infected
210 OVA323-339-pulsed GL261 cells, did not proliferate, indicating that the MHC-II molecules present
211 on infected GL261 cells, did not present antigens to T-cells, reinforcing the MHC-II independence of
212 the observed phenotype. This was further confirmed in the human GB organoid - T-cell co-cultures
213 in the presence of an antigenic pool consisting of cytomegalo-, parainfluenza, and influenza virus
214 peptides ("CPI pool"). No difference in tumor cell death was observed between pulsed and
215 unpulsed co-cultures (**Fig.5B**).

216 To address the transgene specificity of the observed phenotype, we infected P3 organoids with an
217 Ad-GFP vector (**Fig.5C**). Unlike Ad-CIITA, Ad-GFP did not lead to tumor cell death upon co-culture
218 with PBMCs (**Fig.5D**). The same results were obtained in the T16 co-culture model (**Supplementary**
219 **Fig.5A-B**), confirming the selectivity of the immune-mediated phenotype toward CIITA.

220 Next, we determined whether tumor killing required cell-to-cell contact by performing co-cultures
221 in a two-layer transwell system. While we observed the expected reduction in organoid growth due
222 to AdV infection, organoid breakdown in the presence of Ad-CIITA and Ad-CIITA mutant was
223 completely abolished (**Fig.5E**). This was replicated in T16 organoids (**Supplementary Fig.5C**),
224 indicating that immune cells require direct cell-to-cell interaction with target GBs to effectively
225 induce tumor cell death.

226

227 **Immune-mediated tumor cell killing of GB organoids is not induced by degranulating T-cells or by**
228 **activation of death receptor signaling pathways.**

229 We next aimed to assess different modes of contact-dependent T-cell-mediated cell killing.
230 Cytotoxic T-cells conventionally release lytic granules, such as perforin and granzymes, into the
231 immunological synapse. T-cell degranulation did not appear to be involved in CIITA-mediated killing,
232 as evidenced by the absence of the degranulating marker CD107a and intracellular IFN-γ expression
233 (**Fig.6A**). Cell death can also be induced via activation of death receptor signaling in target cells,
234 including tumor necrosis factor alpha (TNF-α)/TNF-receptor (TNF-R) and Fas/Fas ligand (FasL)[18].
235 Blocking these death pathways via anti-human TNF-R and FasL monoclonal antibodies did not
236 impact the ability of CIITA to induce GB organoid killing (**Fig.6B**), in contrast to Actinomycin D- and
237 dimethyl sulfoxide (DMSO)-induced cell killing, respectively (**Supplementary Fig.6**).

238 In an attempt to identify non-classical T-cell activation mechanisms, we investigated the secretion
239 of cytokines upon tumor cell killing mediated by wild-type CIITA at 72 hours post co-culture (**Fig.6C**).

240 We detected increased secretion of the extracellular matrix metalloproteinase inducer (EMMPRIN)
241 and RANTES (Regulated upon Activation, Normal T-cell Expressed, and Secreted) in Ad-CIITA co-
242 culture medium and a decrease in the levels of IL-1alpha, IL-18, VEGF, and IL-6. To what extent such
243 changes in cytokine levels are functionally linked to tumor cell killing remains to be determined.

244

245 **DISCUSSION**

246 CIITA is the master regulator of MHC-II expression, and this biological function has been exploited
247 to trigger adaptive immunity against tumors[19]. Given the need to develop new strategies against
248 GB tumors, we equipped a non-lytic AdV with the wild-type *CIITA* transgene (Ad-CIITA). At basal
249 level, GB tumor cells generally lacked MHC-II expression, while other components of the MHC-II
250 transcriptional machinery were present. Indeed Ad-CIITA infection of primary GB cells resulted in
251 robust MHC-II expression at the surface of infected cells.

252 We found that while Ad-CIITA infection has limited impact on tumor cell growth, effective killing of
253 infected GB organoids is activated and maintained only in the presence of immune cells. Our study
254 reveals a new ability of CIITA to activate T-cells which is independent of MHC-II molecules and
255 antigen presentation. Firstly, we find that a novel CIITA mutant, unable to induce MHC-II still
256 triggers T-cell mediated tumor cell death. Secondly, depletion of either $CD4^+$ or $CD8^+$ cells did not
257 impair immune-mediated cell death. Thirdly, cell killing was independent of antigen presentation.
258 A direct influence of the virus could be ruled out by the use of control empty and GFP-containing
259 vectors. Cell-to-cell contact between target GB and immune cells was necessary, yet, we did not
260 detect evidence of canonical T-cell degranulation or known death signaling pathways. The
261 mechanism by which CIITA induces an MHC-II independent immune-mediated tumor cell death
262 remains to be determined.

263 The newly generated *CIITA* mutant harbors a point mutation (G1088A) within the carboxy-terminal
264 region (4th LRR domain) of an otherwise full-length protein. The replacement of the non-polar, small
265 amino acid glycine with arginine, may impact protein folding, stability and binding properties[20].
266 While wild-type CIITA protein is distributed between the nucleus and cytoplasm[7], the G1088A
267 mutant protein was effectively excluded from the nucleus, in line with a previous report[21]. Our
268 novel point-mutated CIITA variant may thus effectively serve to unravel MHC-II-dependent and -
269 independent activities of CIITA. Cytoplasmic effects of CIITA have been previously reported such as
270 the L1035P CIITA mutant enhancing human immunodeficiency virion maturation through Gag
271 processing by the viral protease[22].

272 The cytotoxicity induced by both Ad-CIITA and Ad-CIITA mutant in patient-derived GB cells was
273 primarily mediated by $CD3^+$ T-cells, in line with *in vivo* results in mice[12, 13,11]. Nevertheless, an
274 involvement of other immune components, such as natural killer cells or macrophages, cannot be
275 currently excluded. Further investigation should also be directed in validating the anticancer role
276 of wild-type and mutant CIITA in humanized GB models.

277 T-cell activation and proliferation commonly require at least two key events: (i) T-cell receptor (TCR)
278 binding to a specific MHC-restricted antigen, and (ii) the interaction of costimulatory molecules on
279 the surface of T-cells and APCs. We have shown that the killing phenotype relies on direct cell-to-
280 cell interaction between the target tumor organoids and the immune cells and was observed

281 despite the absence of CD80 and CD86 costimulatory molecules, which is in line with previous
282 reports[8, 12, 13].

283 A protein cytokine array revealed increased secretion of EMMPRIN and RANTES along with a
284 decrease in various pro-inflammatory cytokines in Ad-CIITA co-culture medium. EMPPRIN is a
285 glycoprotein expressed and secreted by various cell types, including lymphocytes and tumor cells,
286 involved in metalloproteinase induction, energy metabolism, T-cell activation, co-stimulation, and
287 proliferation[23]. RANTES (CCL5) is a potent proinflammatory chemokine that acts as a
288 chemoattractant or immune cell activator[24]. RANTES-induced T-cell activation has various effects,
289 including lymphocyte proliferation or apoptotic cell death, as well as the release of pro-
290 inflammatory cytokines[24]. Further studies are warranted to fully understand the implications of
291 soluble EMMPRIN and RANTES in the observed T-cell-mediated killing.

292 In conclusion, our findings highlight the potential of viral delivery of the *CIITA* transgene in human
293 GB as a promising immunotherapeutic approach for enhancing adaptive responses against GB. The
294 observed T-cell-mediated cytotoxicity, which appears to be largely independent of MHC-II antigen
295 presentation, opens up new avenues for CIITA analysis beyond its canonical transcriptional activity.

296

297 **MATHERIALS AND METHODS**

298 **Patient-derived preclinical models and cell culture.**

299 PDOX models, PDOX-derived *ex vivo* organoids, and PDOX-derived GSC lines were generated as
300 described in[25 26]. DsRed-expressing organoids were created as described in[27]. BG5, BG7, GG16, GG6,
301 U251, and U87 were kindly provided by Prof. Rolf Bjerkvig, University of Bergen; NCH421, NCH465,
302 and NCH644 by Prof. Christel Herold-Mende, University of Heidelberg; and GL261 by Prof. Roberto
303 Accolla, University of Insubria.

304 **HLA typing.**

305 gDNA extracted from GB organoids with the DNeasy Blood & Tissue Kit (Qiagen, Cat# 69504), was
306 sequenced at 11 HLA loci (MHC-I *HLA-A*, *-B*, *-C*; MHC-II *HLA-DRB1/3/4/5*, *-DQA1*, *-DQB1*, *-DPA1*, -
307 *DPB1*) using the Illumina TruSight HLA v2 Sequencing panel (**Table S3**).

308 **Gene expression analysis.**

309 The expression of CIITA and MHC-II associated genes in GB patient tumors and control normal brain
310 was investigated with GEPIA2[28]. To examine gene expression in single cells isolated from GB patient
311 tumors, we exploited the GBap dataset[29] and the DotPlot function of Seurat package. Gene
312 expression in preclinical models was assessed with the Gene-Chip® Human Gene 1.0 ST Arrays
313 (Affimetrix, Cat# 901086) as described previously[26] or RNA-seq on bulk tissue (50 million
314 reads/sample, 2x150bp), using the Illumina Stranded mRNA prep kit on an Illumina NovaSeq 6000
315 sequencer.

316 **Peripheral blood lymphocytes.**

317 Allogeneic PBMCs were isolated from healthy human donor blood (Luxembourg Red Cross) via
318 density gradient centrifugation and cryopreserved. Allogeneic HLA-matched PBMCs were
319 purchased from Immunospot based on their HLA matching (**Table S3**). T-cell populations were

320 isolated from PBMCs using $CD3^+$ (BioLegend, Cat# 480022), $CD4^+$ (Miltenyi, Cat# 130-096-533) or
321 $CD8^+$ (Miltenyi, Cat# 130-096-495) negative isolation kits. PBMC composition and purity were
322 evaluated using multi-color flow cytometry (**Table S2**).

323 Immune cells were cultured in "T-cell medium": RPMI 1640 GlutaMAX™ (Thermo Fisher,
324 Cat#61870036), 9% FBS, 1% human serum (Sigma-Aldrich, Cat#H3667), 0.1 mM Sodium Pyruvate
325 (Thermo Fisher, Cat#11360070), 55 µM β-Mercaptoethanol (Thermo Fisher, Cat#21985023), 1X
326 NEAAs, 5 mM HEPES (Thermo Fisher, Cat#15630080), and 100 U/mL penicillin–streptomycin.

327 **AdV vectors.**

328 Replication-deficient (ΔE1-E3) serotype 5 AdV vectors were created according to the Ad-Easy-1
329 protocol[30]. The AdVs used in the study include Ad-null (no transgene), Ad-GFP, Ad-CIITA (wild-type
330 *CIITA* encoding for MHC-II TransActivator isoform III [NP_000237.2, 1130 aa]), and Ad-CIITA mutant
331 (mutated version of *CIITA*). For all vectors, transgene expression was regulated via the CMV
332 promoter. AdV particles were purified with the Adeno-X™ Mega Purification Kit (Takara, Cat#
333 631032) and titrated using the Adeno-X Rapid Titer kit (Takara, Cat# 632250), following
334 manufacturer's instructions.

335 AdV infection was conducted during cell seeding. After infection, cells were gently shaken at 37°C
336 for up to one hour, and then incubated at 37°C for a maximum of six days post-infection, depending
337 on the read-out.

338 **AdV-infected GB organoid - immune cell co-culture.**

339 Cryopreserved GB single cells were seeded ($2E10^4$ cells/well) in 96-well, Nunclon Sphera-Treated,
340 U-Shaped-Bottom, ultra-low attachment microplates (Thermo Fisher, Cat# 174929), infected in a
341 final volume of 100 µL organoid medium, and incubated at 37°C on an orbital shaker at 40-50 rpm.
342 Three days post-seeding/infection, cryopreserved immune cells were added at different T:E ratios
343 (1:1, 1:5, 1:10). Before co-culture, GB organoids were pulsed with "CPI pool" (ImmunoSpot, Cat#
344 CTL-CPI-001) as a positive control for T-cell activation. Co-cultures were performed in the presence
345 of 25 U/mL IL-2 (Miltenyi, Cat# 130-097-745) and 5 µg/mL anti-CD28 antibody (BioLegend, Cat#
346 302902). Tumor cell viability was monitored in real-time using IncucyteS3, or via flow cytometry at
347 72 hours post-co-culture via staining of $CD45^-$/$CD3^-$/ $CD90^+$ tumor cells with Live/Dead fixable Near-
348 IR (**Table S4**). To study contact-dependency, co-cultures were carried out using transwell-96 with
349 0.4 µm pore polyester membrane inserts (StemCell Technologies, Cat# 100-0419).

350 **Incucyte S3 live cell imaging system.**

351 Incucyte S3 (RRID:SCR_023147) was used to monitor tumor cell viability over time (4X
352 magnification). Organoids were imaged daily for the first 3 days post-seeding/infection and every 4
353 hours after co-culture with immune cells. Data were analyzed using Incucyte 2022A software.

354 To quantify tumor cell viability in dsRed-expressing organoids (P3dsRed and T16dsRed), we
355 monitored total integrated red fluorescence intensity (RCU x μm^2/Image) over time. For T188 tumor
356 cells transiently labeled with 0.3 µM of Incucyte® Cytolight Rapid Red Dye (Sartorius, Cat# 4706),
357 we measured the red total area (μm^2/Image) over time.

358 **Degranulation assay.**

359 At 24 hours post co-culture (T:E ratio of 1:10), $CD3^+$ T-cells were labelled with anti-CD107a antibody
360 (**Table S4**). Freshly thawed $CD3^+$ T-cells stimulated with 50 ng/mL phorbol 12-myristate 13-acetate
361 (PMA) (Enzo Life Sciences, Cat# BML-PE160-0001) and 1 µg/mL ionomycin (Enzo Life Sciences, Cat#
362 ALX-450-007-M001) were used as positive control. Cells were then incubated for 4 hours at 37°C
363 with GolgiStop™ (BD, Cat#554724, 1:1000 dilution), and GolgiPlug (BD, Cat#555029, 1:500 dilution).
364 $CD3^+$ T-cells from five different wells (~1 million cells) were pooled together, stained with cell
365 surface markers for 30 minutes at 4°C, fixed/permeabilized with Cytofix/Cytoperm (BD,
366 Cat#554714) for 20 min at 4°C, and finally incubated with anti-IFN-γ intracellular antibody for 30
367 minutes at 4°C (**Table S4**).

368 ***In vitro* T-cell proliferation assay**

369 GL261 cells were infected and pulsed with two concentrations (50 µg/ml and 100 µg/ml) of
370 OVA323-339 (Eurogentec, Cat#AS27024) for 4 hours at 37°C. After extensive washes, they were co-
371 cultured with Cell Trace Violet (Thermo Fisher, Cat#C34557)-stained CD3+ T-cells from OT-II mice.
372 As a positive control, bone marrow-derived macrophages were also pulsed with OVA323-339 and
373 co-cultured with OT-II CD3+ T-cells. CD3+ T-cells were acquired using the NovoCyte Quanteon Flow
374 Cytometer on day 0 (before co-culture) and on day 4 (four days post-co-culture) to trace $CD4^+$ T-cell
375 proliferation.

376 **Neutralization assay.**

377 Organoids were treated with increasing concentrations of anti-human TNF-RI/TNFRSF1A (R&D,
378 Cat# MAB225) (0.16 µg/mL, 0.08 µg/mL, 0.04 µg/mL, and 0.02 µg/mL) and anti-human Fas
379 Ligand/TNFSF6 (R&D, Cat# MAB126) (20 ng/mL, 10 ng/mL, 5 ng/mL, and 2.5 ng/mL) monoclonal
380 antibodies (**Table S4**). Organoids treated with actinomycin D (1 µg/mL) or 2.5% DMSO were used
381 as positive controls for TNF-R and FasL neutralization, respectively. Immune cell-mediated tumor
382 killing was assessed via Incucyte S3.

383 **Measurement of cytokine secretion.**

384 At 72 hours post PBMC co-culture (T:E ratio of 1:10), conditioned media were collected,
385 centrifuged, and screened using the Proteome Profiler Human XL Cytokine Array Kit (R&D, Cat#
386 ARY022B). Array membranes were then exposed to X-Ray films (1, 5, and 10 minutes). The average
387 signal (pixel density) per analyte was quantified using Quick Spots software.

388 **Quantitative RT–PCR.**

389 Total RNA was extracted using the RNeasy Mini Kit (Qiagen, Cat# 74104), reverse-transcribed to
390 cDNA using Fast SYBR Green (Thermo Fisher, Cat# 4385612), and QuantStudio 5 Real-Time PCR
391 System (RRID:SCR_020240). Relative gene expression levels were calculated through the ΔCT
392 method by using *elongation factor 1 alpha (EF1α)* as a housekeeping gene. The primers used were
393 as follows: CIITA (Fw: TTATGCCAATATCGCGGAACTG, Rv: CATCTGGTCCTATGTGCTTGAAA), HLA-DRα (Fw:
394 AGTCCCTGTGCTAGGATTTTTCA, Rv: ACATAAACTCGCCTGATTGGTC), EF1α (Fw:
395 TTGTCGTCATTGGACACGTAG, Rv: TGCCACCGCATTTATAGATCAG), and GAPDH (Fw:
396 CTCCCACTCTTCCACCTTCG, Rv: CCACCACCCTGTTGCTGTAG).

397 **Immunofluorescence.**

398 Cells were seeded/infected (5E10^4 cells/well) in 8-well µ-slides (Ibidi, Cat# 80826) and, three days
399 post-infection, were fixed with 4% PFA for 15 minutes at RT and blocked in 1X PBS with 0.5% Triton
400 X-100 (Thermo Fisher, Cat# 85111) and 10% FBS for 1 hour at RT. Cells were then incubated with
401 anti-CIITA primary antibody (Abcam, Cat# ab92511) diluted in 1X PBS with 0.5% Triton X-100
402 overnight at 4°C (**Table S4**). After three washes in 1X PBS, the cells were incubated with Alexa Fluor
403 488 secondary antibody (Thermo Fisher, Cat# A11001) and Hoechst dye (Thermo Fisher, Cat#
404 H3569) diluted in 1X PBS with 0.01% BSA (Sigma-Aldrich, Cat# A9418) for 1 hour at RT (**Table S4**).
405 Cells were then imaged with a Zeiss LSM 880 Confocal Laser Scanning Microscope
406 (RRID:SCR_020925) and Zen Blue software (RRID:SCR_013672).

407 **Flow cytometry.**

408 Single cells were stained with fluorochrome-conjugated antibodies (**Table S4**) diluted in ice-cold 1X
409 PBS with 0,2% BSA ("FACS buffer") or Brilliant Stain Buffer ("BV buffer") (BD, Cat# 563794) for 30
410 minutes at 4°C in the dark. Stained cells (1 million cells in 100 µL, we scaled down accordingly for a
411 smaller number of cells) were acquired with NovoCyte Quanteon Flow Cytometer. Data were
412 analyzed using FlowJo (RRID:SCR_008520) version 10.

413 **Statistical analysis.**

414 Experimental results were analyzed using GraphPad Prism 9 (RRID:SCR_002798) and reported as
415 mean ± standard deviation (SD) or, for co-culture experiments, as mean ± standard error of mean
416 (SEM). For flow cytometry results, figures depict expression curves, along with the mean
417 percentage of positive cells and their standard deviation (based on three independent
418 experiments). All means were calculated based on a minimum of three independent experiments.
419 For co-culture experiments, all means were calculated based on a minimum of three immune cell
420 donors, representing three different biological replicates. One-way ANOVA was employed to
421 compare multiple groups, while two-way ANOVA was used to compare two or more factors
422 simultaneously. A P value < 0.05 was used to determine statistical significance.

423

424 **FIGURES**

425 **Figure 1. Expression of *MHC-II*-related transcripts in human glioblastoma and associated models.**
426 **A**. Bulk RNA-seq gene expression in GB patient tumors (n=163) versus control normal brain (n=207).
427 *p<0.01 (one-way ANOVA). **B.** Single-cell RNA-seq gene expression in GB patient tumors. **C.**
428 Heatmap representing bulk RNA-seq (human specific) gene expression in GB PDOXs. Grey color
429 indicates lack of expression. PDOX replicates are indicated by numbers. **D.** FACS analysis of surface
430 MHC-II (anti-HLA-DR/DP/DQ-FITC), in control conditions (cells unstained or mock-stimulated) and
431 upon IFN-γ stimulation.

432 **Figure 2. Characterization of Ad-CIITA and Ad-CIITA mutant in human glioblastoma stem-like cells**.
433 **A**. AdV vectors used in the study. **B-D**. Virus quality check in human P3NS and T16NS infected at
434 MOI 50. mRNA (**B**) and protein levels (**C**) of CIITA and HLA-DRα were analyzed 72 hours post-
435 infection by qRT–PCR and Western blot, respectively. qRT–PCR was normalized to Ef1a, while
436 Western blot to GAPDH. Mean ± SD. ****p<0.0001 (one-way ANOVA). **D**. FACS analysis of surface
437 MHC-II (anti-HLA-DR/DP/DQ-FITC) at 72 hours and 6 days post-infection.

438 **Figure 3. Successful infection of human primary glioblastoma organoids by adenoviral vectors. A.**
439 Western Blot analysis of CIITA and HLA-DRα expression at 72 hours post-infection in P3 organoids.
440 **B.** Representative H&E (top) and anti-HLA-DRα (bottom) staining at 72 hours post-infection (MOI
441 50). **C.** FACS analysis of surface MHC-II (anti-HLA-DR/DP/DQ-FITC) at 72 hours and 6-days post-
442 infection (MOI 50). **D.** Evaluation of virus-mediated cytotoxicity (P3dsRed) via Incucyte S3. Mean ±
443 SEM.

444 **Figure 4. Immune cell-mediated tumor cell killing in human primary GB organoids induced by Ad-**
445 **CIITA and Ad-CIITA mutant. A.** Schematic of AdV-infected GB organoids co-cultured with immune
446 cells. **B-C.** Tumor cell viability in P3dsRed organoids (MOI 75): **(B)** alone (no co-culture) or co-
447 cultured with PBMCs; **(C)** co-cultured with $CD3^+$, $CD4^+$ or $CD8^+$ T-cells; Mean ± SEM. *p<0.05,
448 **p<0.01, ***p<0.001, and ****p<0.0001 (two-way ANOVA). **D.** FACS analysis showing the
449 proportion of live/dead cells in $CD90^+$ tumor cells at 72 hours post-co-culture: alone (left), co-
450 cultured with PBMCs (middle), and co-cultured with CD3+ T-cells (right). Mean ± SD. *p<0.05,
451 **p<0.01, ***p<0.001, and ****p<0.0001 (one-way ANOVA). **E.** Tumor cell viability in P3dsRed
452 organoids (MOI 75) co-cultured with HLA-matched PBMCs or $CD3^+$ T-cells. Mean ± SEM. *p<0.05,
453 **p<0.01, ***p<0.001, and ****p<0.0001 (two-way ANOVA).

454 **Figure 5. CIITA expression and cell-to-cell contact, but not antigen presentation, are required for**
455 **immune-mediated tumor cell killing. A.** *In vitro* proliferation assay of $CD3^+$ T-cells co-cultured with
456 OVA323-339-pulsed GL261 tumor cells or BMDM (positive control). **B.** Tumor cell viability in
457 P3dsRed organoids (MOI 75) when co-cultured with $CD3^+$ T-cells (T:E ratio of 1:10), comparing the
458 effects of unpulsed versus CPI pool-pulsed organoids. **C-E.** P3dsRed organoids (MOI 75) co-cultured
459 with PBMCs (T:E - 1:10). **C.** GFP expression in Ad-GFP-infected vs non-infected organoids. Mean ±
460 SD. ****p<0.0001 (two-way ANOVA). **D.** Tumor cell viability in Ad-GFP- or Ad-CIITA-infected GB
461 organoids compared to non-infected control. Mean ± SEM. ****p<0.0001 (one-way ANOVA). **E.**
462 Tumor cell viability in two-layer transwell co-culture model. Mean ± SEM. **p<0.01 (one-way
463 ANOVA).

464 **Figure 6. Immune-mediated tumor cell killing of GB organoids does not involve T-cell**
465 **degranulation or canonical death receptor signaling pathways. A.** FACS analysis of surface CD107a
466 (left panel) and intracellular IFN-γ (right panel) in $CD4^+$ and $CD8^+$ T-cells at 24 hours post co-culture.
467 Mean ± SD. *p<0.05, **p<0.01 and ***p<0.001 (one-way ANOVA). **B.** Neutralization assay using
468 anti-human TNF-R (MAB225) (left panel) or anti-human FasL (MAB126) (right panel). Mean ± SEM.
469 **C.** Heatmap of the most upregulated and downregulated proteins detected via protein cytokine
470 array (bottom left). Graphs showing levels of secreted EMMPRIN and RANTES (bottom right). Mean
471 ± SD.

472

473 **SUPPLEMENTARY FIGURES**

474 **Supplementary Figure 1. MHC-II related gene expression analysis in GB patient tumors and**
475 **human preclinical models. A.** Heatmap representing gene expression levels in normal human brain,
476 GB patient tumors, PDOXs, GSC lines (NCH421k, NCH644), and classical glioma lines (U87, U251)
477 grown *in vitro* or *in vivo* as xenograft ('X'). Lack of expression is represented by grey color. Human
478 specific arrays were applied for transcriptome analysis. **B.** FACS analysis of surface MHC-II (anti-

479 HLA-DR/DP/DQ-FITC) in control conditions (cells unstained or mock-stimulated) and upon IFN-γ
480 stimulation.

481 **Supplementary Figure 2. Characterization of wild-type and mutant CIITA adenoviral vectors in**
482 **adherent human (U251) and murine (GL261) cell lines. A.** Sanger sequencing results of the wild-
483 type vs mutant *CIITA* DNA. **B.** PyMOL representation of the amino acid string surrounding position
484 1088 in wild-type (left) and mutated (right) CIITA. **C.** Representative confocal images of CIITA (Alexa
485 Fluor 488) in U251 at 72 hours post-infection (magnification 63X). CIITA cellular distribution was
486 quantified by measuring the ratio of cytoplasmic-to-nuclear fluorescence intensity. Mean ± SD.
487 ****p<0.0001 (two-way ANOVA). **D-F.** Ad-CIITA characterization in GL261. **D.** FACS analysis of MHC-
488 II (anti-IA-IE-PerCP) at increasing Ad-CIITA MOIs. **E.** mRNA (left) and protein (right) levels of CIITA at
489 48 and 72 hours post-infection, as analyzed by qRT–PCR and Western blot, respectively. qRT-PCR
490 and WB results were normalized to GAPDH. Mean ± SD. ***p<0.001, ****p<0.0001 (two-way
491 ANOVA).

492 **Supplementary Figure 3. Infection of human primary glioblastoma organoids with adenoviral**
493 **vectors and impact on MHC-I expression. A.** FACS analysis of surface MHC-I (anti-HLA-A/B/C-
494 BV510), CD80 (anti-CD80-PE) and CD86 (anti-CD86-BV421) in P3 organoids. **B.** Tumor cell viability
495 of T16dsRed (top) and red dye-labeled T188 (bottom) organoids infected at increasing virus MOIs.
496 Mean ± SEM.

497 **Supplementary Figure 4. Evaluation of immune cell-mediated tumor cell killing in human primary**
498 **GB organoids. A.** FACS gating strategy to phenotype PBMCs and MACS-purified T-cell fractions. **B-**
499 **C.** Tumor cell viability in T16dsRed (left panel, MOI 25) or red dye-labeled T188 (right panel, MOI
500 75) organoids: **(B)** alone (no co-culture) or co-cultured with PBMCs; **(C)** co-cultured with $CD3^+$, $CD4^+$,
501 or $CD8^+$ T-cells. **D.** Tumor cell viability in T16dsRed organoids (MOI 25) co-cultured with HLA-
502 matched PBMCs or $CD3^+$ T-cells. Mean ± SEM. *p<0.05, **p<0.01, ***p<0.001, and ****p<0.0001
503 (two-way ANOVA). Deviations from virus MOI are explicitly indicated on the graph.

504 **Supplementary Figure 5. Requirement for CIITA expression and immune-tumor cell contact, but**
505 **not antigen presentation. A-C.** T16dsRed organoids (MOI 25) co-cultured with PBMCs (T:E - 1:10).
506 **A.** GFP expression in Ad-GFP-infected vs non-infected organoids. Mean ± SD. ****p<0.0001 (two-
507 way ANOVA). **B.** Tumor cell viability in Ad-GFP- or Ad-CIITA-infected GB organoids compared to non-
508 infected control. Mean ± SEM. *p<0.05, **p<0.01 (one-way ANOVA). **C.** Tumor cell viability in two-
509 layer transwell co-culture model. Mean ± SEM.

510 **Supplementary Figure 6. Positive controls of neutralization assay.** Actinomycin D- and DMSO-
511 induced tumor cell death blocked by anti-human TNF-R (MAB225) (left panel) and anti-human FasL
512 (MAB126) (right panel), respectively. Mean ± SEM.

513

514 **ACKNOWLEDGEMENTS:** We are grateful for the use of the LIH PRECISION-PDX Brain Tumor Bank
515 (www.precision-pdx.lu), supported by the patients, the Neurosurgery Department of the Centre
516 Hospitalier de Luxembourg, the NORLUX Neuro-Oncology Laboratory and the Clinical and
517 Epidemiological Investigation Center of LIH. We thank Prof. Roberto Accolla and Prof. Greta Forlani
518 for providing cell lines and critically reviewing the manuscript, Pilar M. Moreno-Sanchez for
519 technical assistance in the management of PDOXs, and the Luxembourg Croix Rouge and its donors

for generously providing healthy donor blood samples. We acknowledge the support from LIH's core facilities (Animal facility, In vivo imaging facility, National Cytometry Platform, LUXGEN sequencing platform).

AUTHOR CONTRIBUTION: Conceptualization (I. S., A.P. A.G., S.P.N., A.M.), methodology (I.S., E.K., A.P., M.R., A.C., A.G.), investigation (I.S., E.K., A.P., M.R., A.L., A.O., V.B., G.M.D.), formal analysis (L.E., B.N., A.G.), supervision (A.P., A.G., A.M., S.P.N.) writing - original draft (I.S., A.G., A.M., S.P.N.), revision (I.S., E.K., A.G., S.P.N.) – review & editing (all authors). The authors approved the final version of the manuscript as submitted and agreed to be accountable for all the aspects of the work.

CONFLICT OF INTEREST: The authors have nothing to disclose.

FUNDING INFORMATION: We acknowledge the financial support by the Luxembourg Institute of Health, FNRS-Télévie (GBodImm no. 7.8513.18, GBodImm2 no. 7651720F, ImmoGB 7.8505.20, ImmoGB2 7.6603.22) and the Luxembourg National Research Fund (C20/BM/14646004/GLASSLUX, C21/BM/15739125/DIOMEDES).

DATA AVAILABILITY STATEMENT: The authors confirm that the data supporting the findings of this study are available within the article and its supplementary materials.

REFERENCES

1 Pires-Afonso Y *et al*. Revealing and Harnessing Tumour-Associated Microglia/Macrophage Heterogeneity in Glioblastoma. *Int J Mol Sci* 2020; 21.

2 Quail DF *et al*. The Microenvironmental Landscape of Brain Tumors. *Cancer Cell* 2017; 31: 326-341.

3 Woroniecka K *et al*. T-Cell Exhaustion Signatures Vary with Tumor Type and Are Severe in Glioblastoma. *Clin Cancer Res* 2018; 24: 4175-4186.

4 Burster T *et al*. Regulation of MHC I Molecules in Glioblastoma Cells and the Sensitizing of NK Cells. *Pharmaceuticals (Basel)* 2021; 14.

5 Salvato I *et al*. Immunotherapeutic Strategies for the Treatment of Glioblastoma: Current Challenges and Future Perspectives. *Cancers* 2024; 16: 1276.

6 Forlani G *et al*. The NLR member CIITA: Master controller of adaptive and intrinsic immunity and unexpected tool in cancer immunotherapy. *Biomed J* 2023; 46: 100631.

559
560 7 Leon Machado JA *et al*. The MHC Class II Transactivator CIITA: Not (Quite) the Odd-One-
561 Out Anymore among NLR Proteins. *Int J Mol Sci* 2021; 22.

562
563 8 Mortara L *et al*. CIITA-induced MHC class II expression in mammary adenocarcinoma leads
564 to a Th1 polarization of the tumor microenvironment, tumor rejection, and specific
565 antitumor memory. *Clin Cancer Res* 2006; 12: 3435-3443.

566
567 9 Thompson JA *et al*. Tumor cells transduced with the MHC class II Transactivator and CD80
568 activate tumor-specific CD4+ T cells whether or not they are silenced for invariant chain.
569 *Cancer Res* 2006; 66: 1147-1154.

570
571 10 Palma ML *et al*. Development of potent class II transactivator gene delivery systems
572 capable of inducing de novo MHC II expression in human cells, in vitro and ex vivo. *Gene*
573 *Ther* 2017; 24: 342-352.

574
575 11 Celesti F *et al*. Protective anti-tumor vaccination against glioblastoma expressing the MHC
576 class II transactivator CIITA. *Front Immunol* 2023; 14: 1133177.

577
578 12 Meazza R *et al*. Tumor rejection by gene transfer of the MHC class II transactivator in
579 murine mammary adenocarcinoma cells. *Eur J Immunol* 2003; 33: 1183-1192.

580
581 13 Frangione V *et al*. CIITA-driven MHC-II positive tumor cells: preventive vaccines and
582 superior generators of antitumor CD4+ T lymphocytes for immunotherapy. *Int J Cancer*
583 2010; 127: 1614-1624.

584
585 14 Tan AK *et al*. Limited Effects of Class II Transactivator-Based Immunotherapy in Murine
586 and Human Glioblastoma. *Cancers (Basel)* 2023; 16.

587
588 15 Nemerow GR *et al*. Role of alpha(v) integrins in adenovirus cell entry and gene delivery.
589 *Microbiol Mol Biol Rev* 1999; 63: 725-734.

590
591 16 Zheng C *et al*. Adenoviral Vector Cytotoxicity Depends in Part on the Transgene Encoded.
592 *Biochemical and Biophysical Research Communications* 2000; 274: 767-771.

593
594 17 Zhou G *et al*. Modelling immune cytotoxicity for cholangiocarcinoma with tumour-derived
595 organoids and effector T cells. *British Journal of Cancer* 2022; 127: 649-660.

596
597 18 Barry M *et al*. Cytotoxic T lymphocytes: all roads lead to death. *Nat Rev Immunol* 2002; 2:
598 401-409.

599
600 19 Accolla RS *et al*. CIITA-Driven MHC Class II Expressing Tumor Cells as Antigen Presenting
601 Cell Performers: Toward the Construction of an Optimal Anti-tumor Vaccine. *Front*
602 *Immunol* 2019; 10: 1806.

603
604 20 Molnár J *et al*. Characterization of Disease-Associated Mutations in Human
605 Transmembrane Proteins. *PLoS One* 2016; 11: e0151760.

606
607 21 Towey M *et al*. Nuclear localisation of CIITA is controlled by a carboxy terminal leucine-
608 rich repeat region. *Molecular Immunology* 2002; 38: 627-634.

609
610 22 Porter KA *et al*. Class II Transactivator (CIITA) Enhances Cytoplasmic Processing of HIV-1
611 Pr55Gag. *PLOS ONE* 2010; 5: e11304.

612
613 23 Kaushik DK *et al*. Evaluating Soluble EMMPRIN as a Marker of Disease Activity in Multiple
614 Sclerosis: Studies of Serum and Cerebrospinal Fluid. *PLoS One* 2016; 11: e0163802.

615
616 24 Appay V *et al*. RANTES activates antigen-specific cytotoxic T lymphocytes in a mitogen-like
617 manner through cell surface aggregation. *International Immunology* 2000; 12: 1173-1182.

618
619 25 Oudin A *et al*. Protocol for derivation of organoids and patient-derived orthotopic
620 xenografts from glioma patient tumors. *STAR Protoc* 2021; 2: 100534.

621
622 26 Golebiewska A *et al*. Patient-derived organoids and orthotopic xenografts of primary and
623 recurrent gliomas represent relevant patient avatars for precision oncology. *Acta*
624 *Neuropathologica* 2020; 140: 919-949.

625
626 27 Niclou SP *et al*. A novel eGFP-expressing immunodeficient mouse model to study tumor-
627 host interactions. *The FASEB Journal* 2008; 22: 3120-3128.

628
629 28 Tang Z *et al*. GEPIA2: an enhanced web server for large-scale expression profiling and
630 interactive analysis. *Nucleic Acids Research* 2019; 47: W556-W560.

631
632 29 Ruiz-Moreno C *et al*. Harmonized single-cell landscape, intercellular crosstalk and tumor
633 architecture of glioblastoma. *bioRxiv* 2022: 2022.2008.2027.505439.

634
635 30 He T-C *et al*. A simplified system for generating recombinant adenoviruses. *Proceedings of*
636 *the National Academy of Sciences* 1998; 95: 2509-2514.

637

638

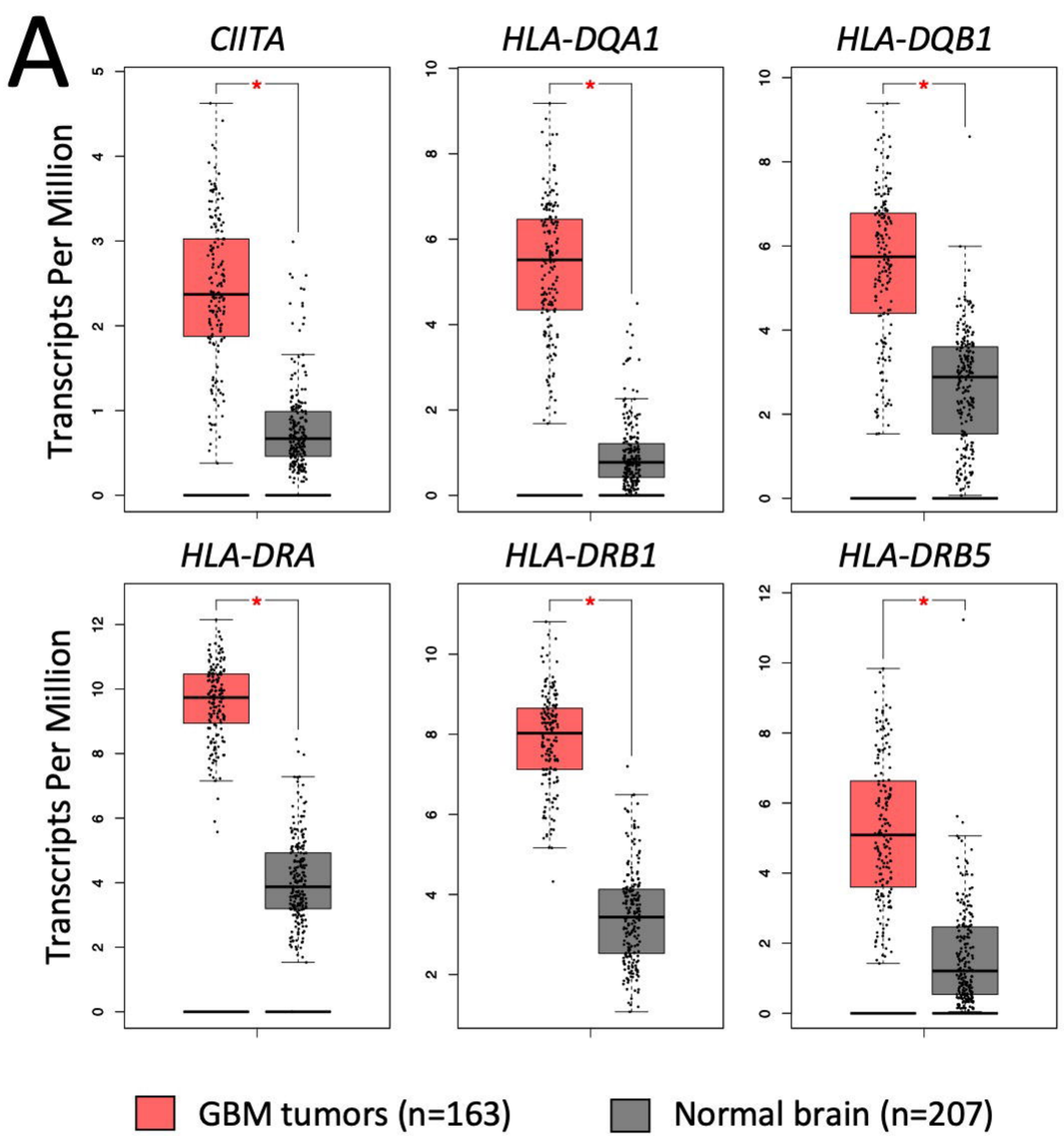

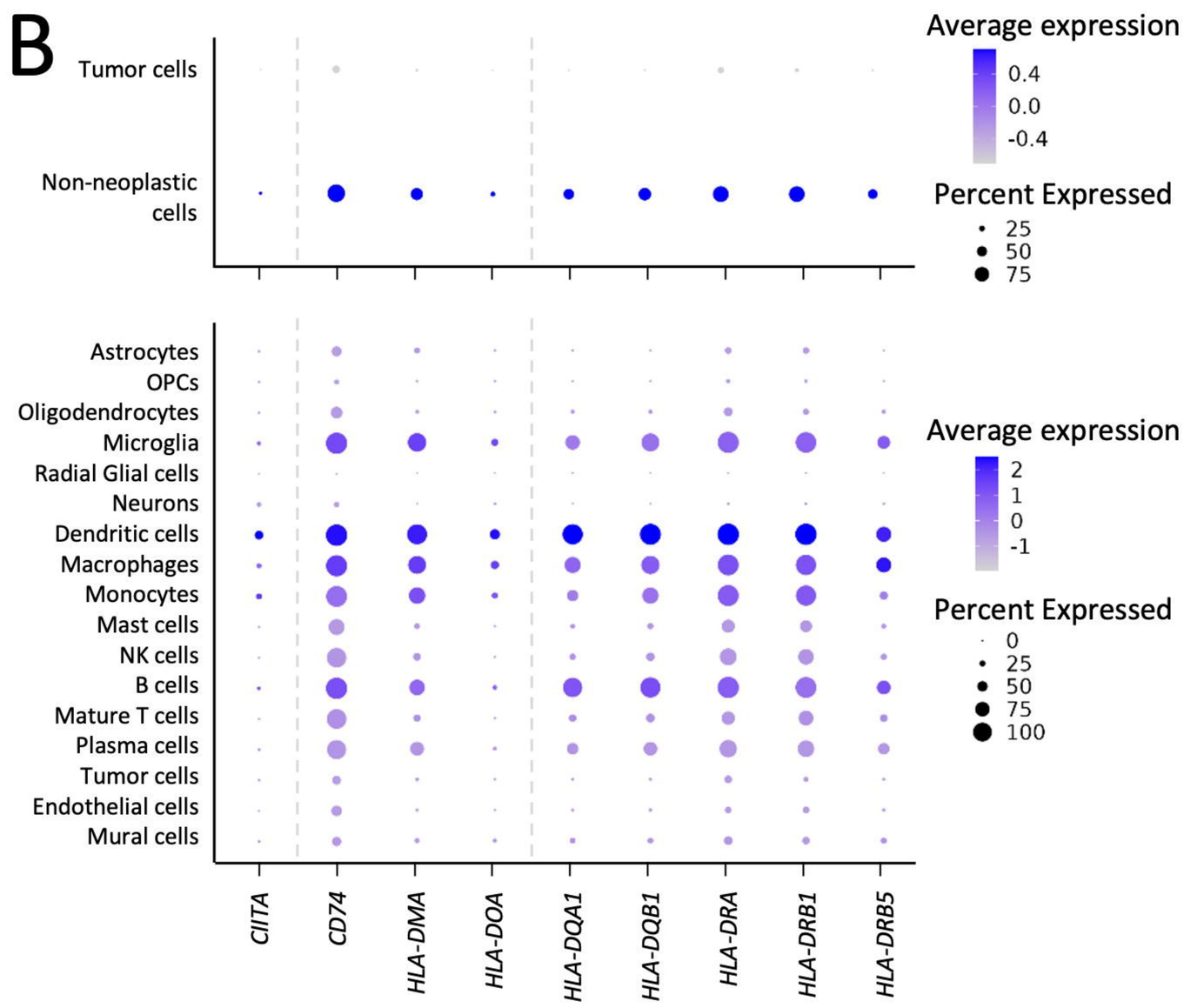

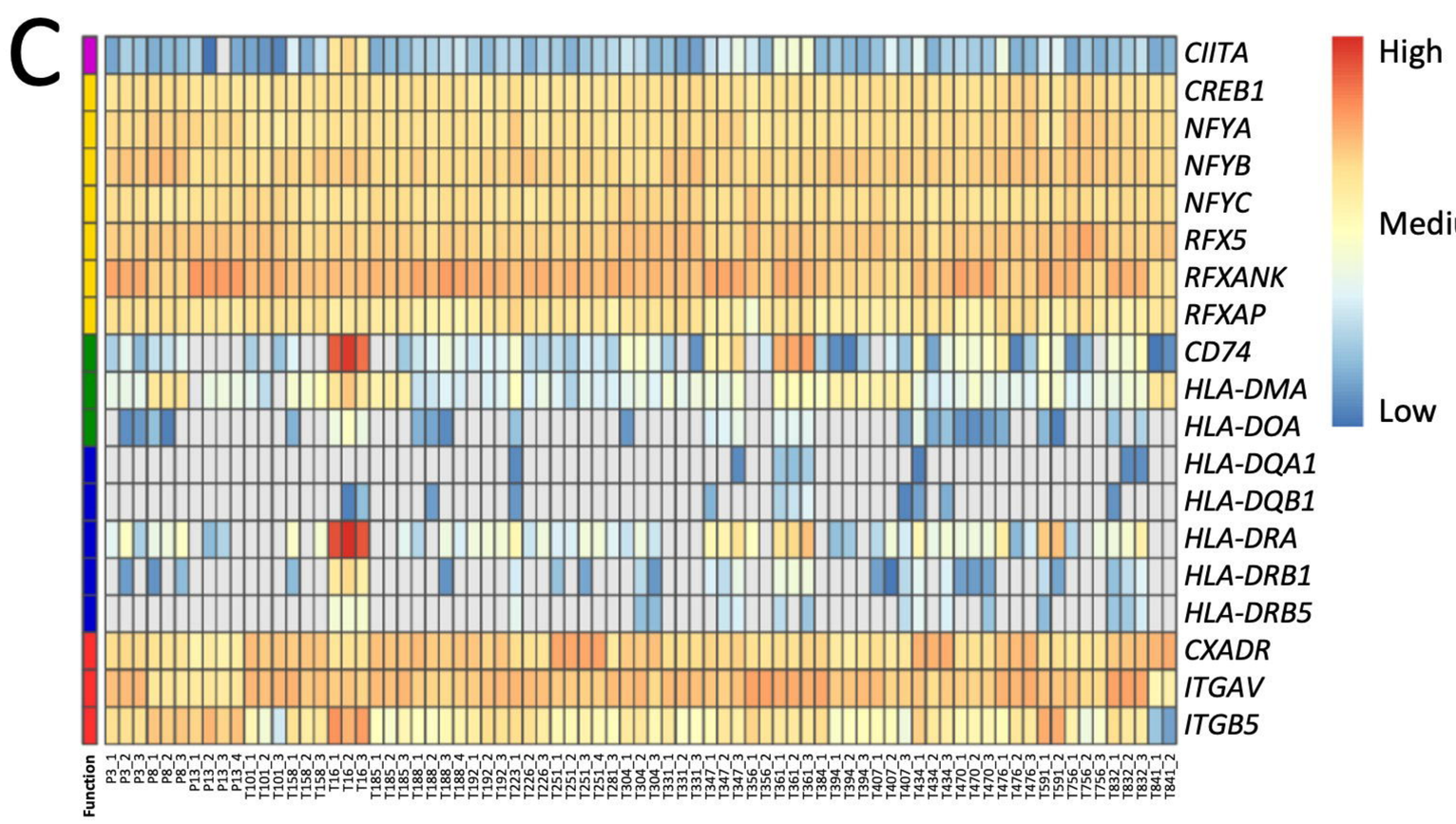

Function

- MHC-II transcriptional regulation
- MHC-II enhanceosome complex
- MHC-II antigen processing
- MHC-II antigen presentation
- Adenovirus infection

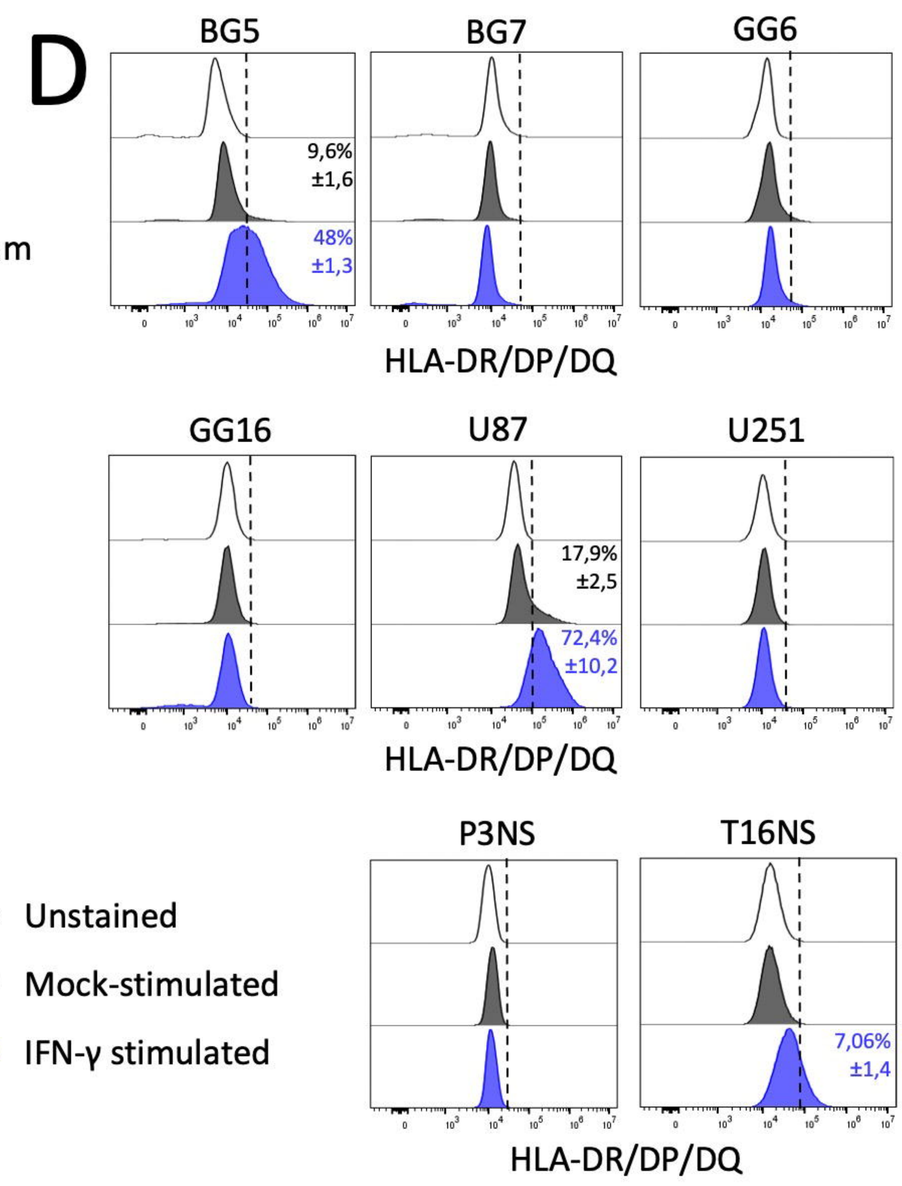

Figure 1

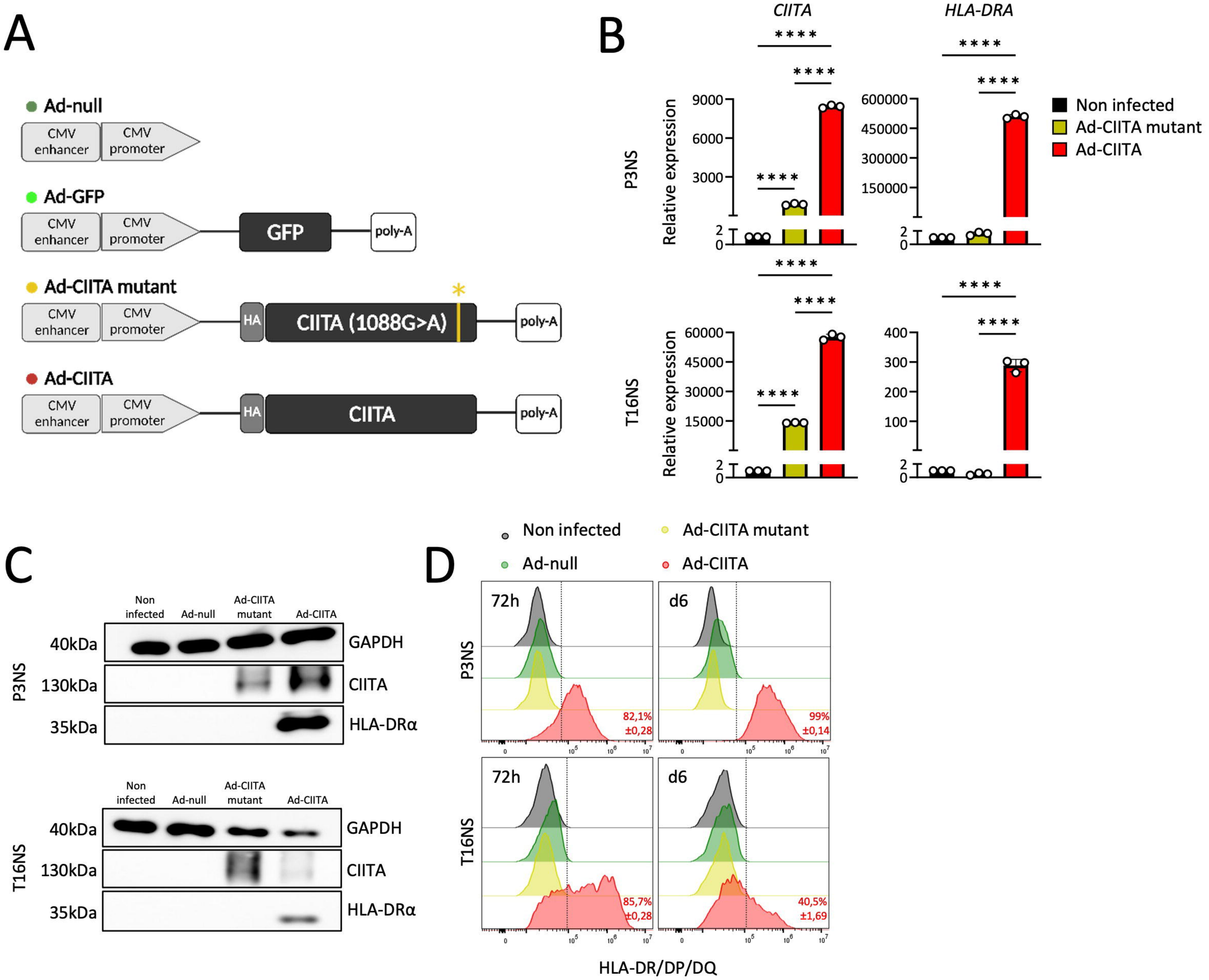
A
Ad-null
CMV enhancer
CMV promoter
Ad-GFP
GFP
poly-A
Ad-CIITA mutant
HA
CIITA (1088G>A)
Ad-CIITA
CIITA
B
CIITA
HLA-DRA
P3NS
T16NS
Relative expression
Non infected
Ad-CIITA mutant
Ad-CIITA
C
Non infected
Ad-null
Ad-CIITA mutant
Ad-CIITA
40kDa
130kDa
35kDa
GAPDH
CIITA
HLA-DRα
D
Non infected
Ad-CIITA mutant
Ad-null
Ad-CIITA
72h
d6
82,1% ±0,28
99% ±0,14
85,7% ±0,28
40,5% ±1,69
HLA-DR/DP/DQ

Figure 2

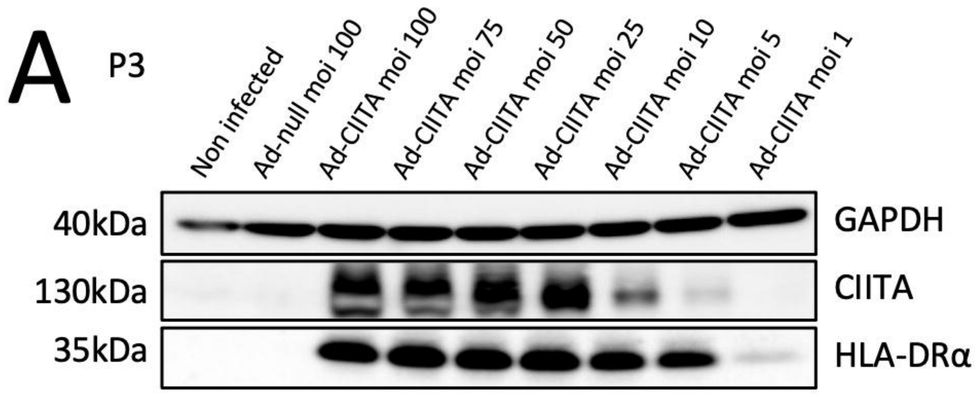
A
P3
Non infected
Ad-null moi 100
Ad-CIITA moi 100
Ad-CIITA moi 75
Ad-CIITA moi 50
Ad-CIITA moi 25
Ad-CIITA moi 10
Ad-CIITA moi 5
Ad-CIITA moi 1
40kDa
GAPDH
130kDa
CIITA
35kDa
HLA-DRα

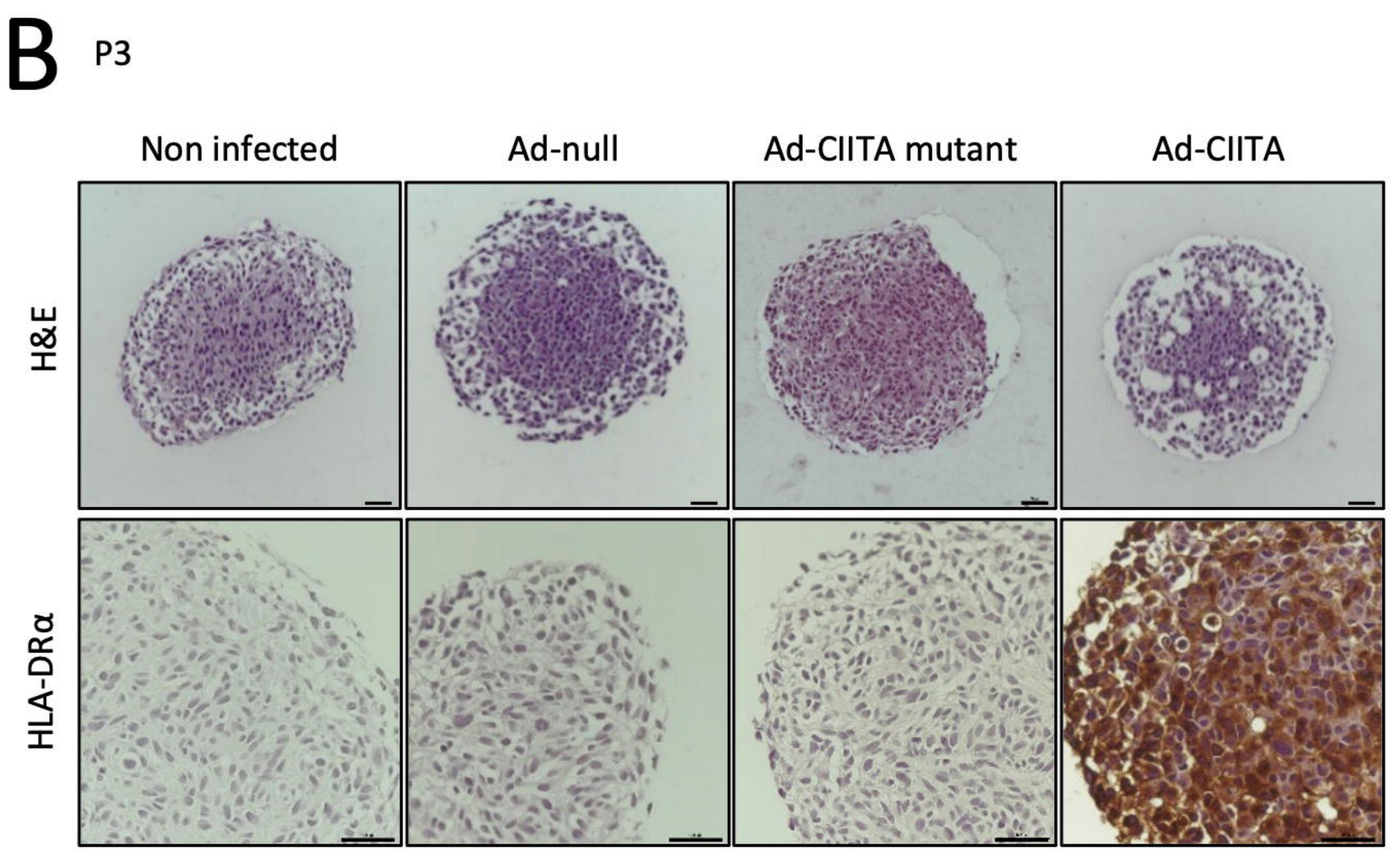
B
P3
Non infected
Ad-null
Ad-CIITA mutant
Ad-CIITA
H&E
HLA-DRα

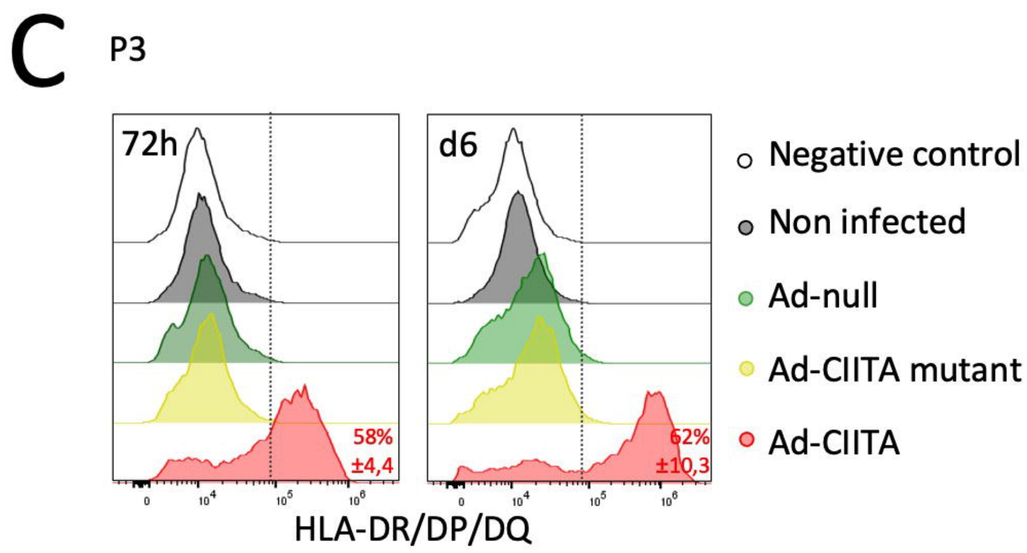
C
P3
72h
d6
58%
±4,4
62%
±10,3
HLA-DR/DP/DQ
Negative control
Non infected
Ad-null
Ad-CIITA mutant
Ad-CIITA

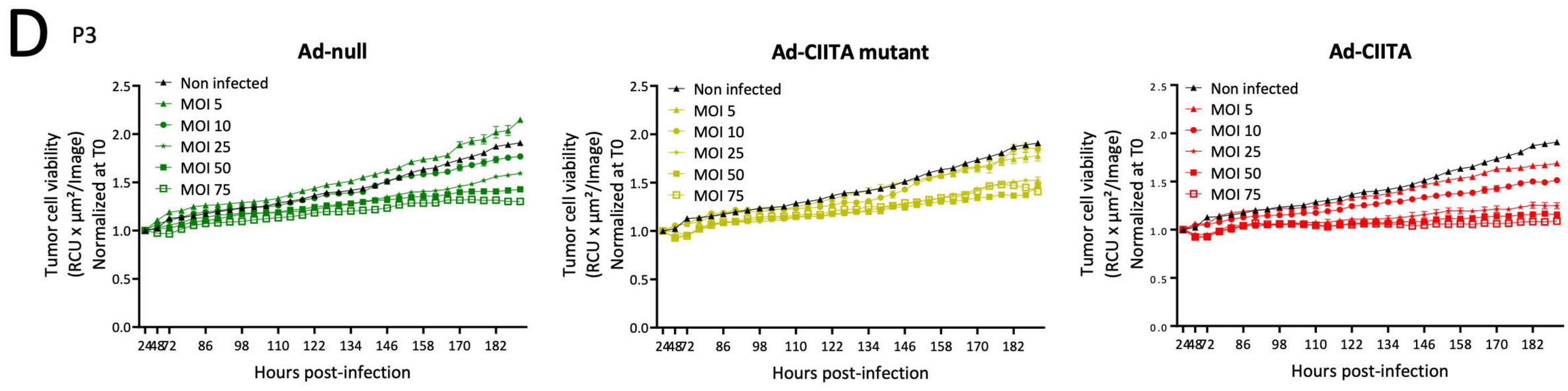
D
P3
Ad-null
Ad-CIITA mutant
Ad-CIITA
Non infected
MOI 5
MOI 10
MOI 25
MOI 50
MOI 75
Tumor cell viability
(RCU x µm²/Image)
Normalized at T0
Hours post-infection

Figure 3

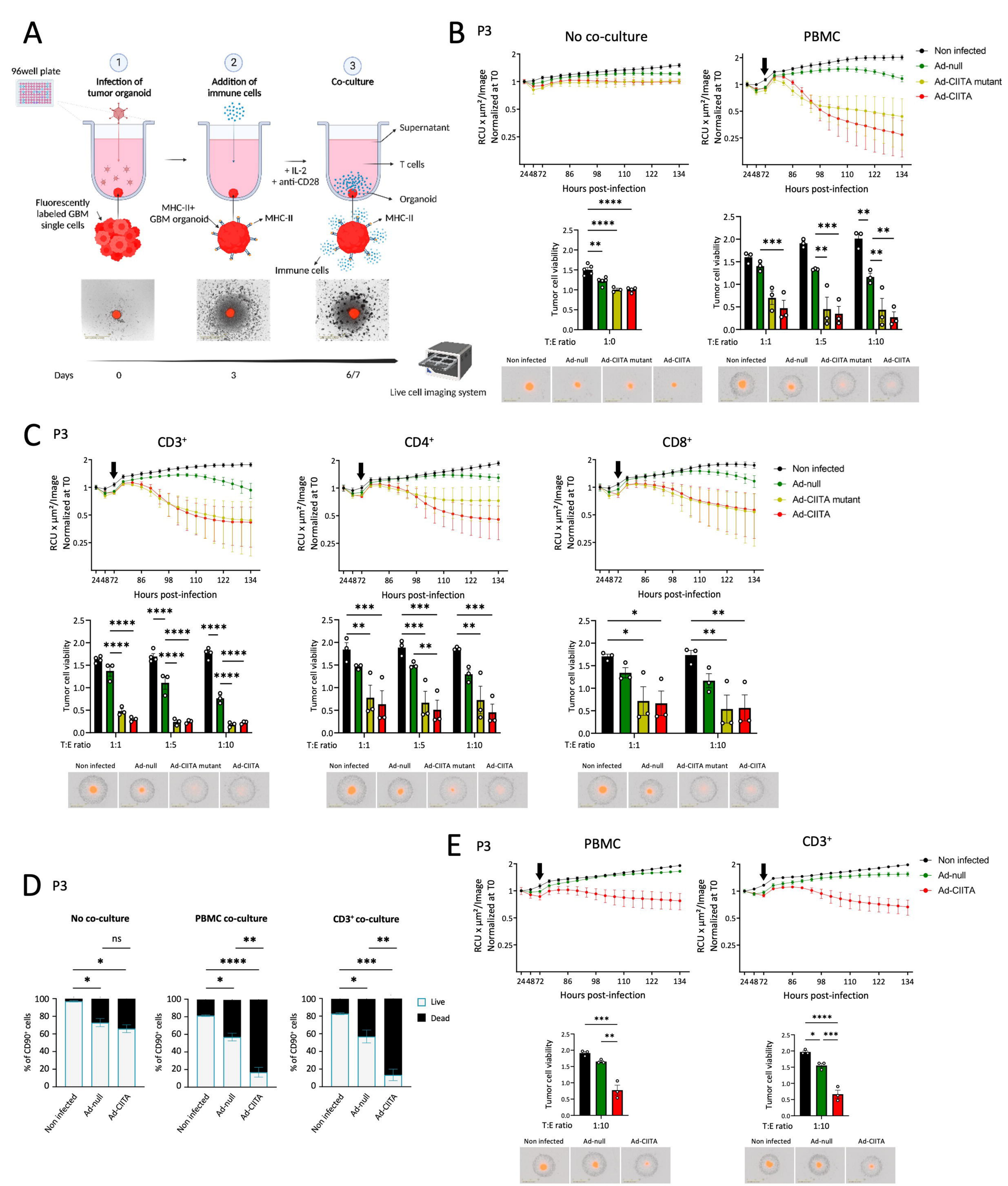
A
96well plate
1
Infection of tumor organoid
2
Addition of immune cells
3
Co-culture
Supernatant
T cells
+ IL-2
+ anti-CD28
Organoid
Fluorescently labeled GBM single cells
MHC-II+ GBM organoid
MHC-II
MHC-II
Immune cells
Days
0
3
6/7
Live cell imaging system
B
P3
No co-culture
PBMC
Non infected
Ad-null
Ad-CIITA mutant
Ad-CIITA
RCU x µm²/Image Normalized at T0
Hours post-infection
Tumor cell viability
T:E ratio
1:0
1:1
1:5
1:10
C
P3
CD3+
CD4+
CD8+
D
P3
No co-culture
PBMC co-culture
CD3+ co-culture
% of CD90+ cells
Live
Dead
E
P3
PBMC
CD3+

Figure 4

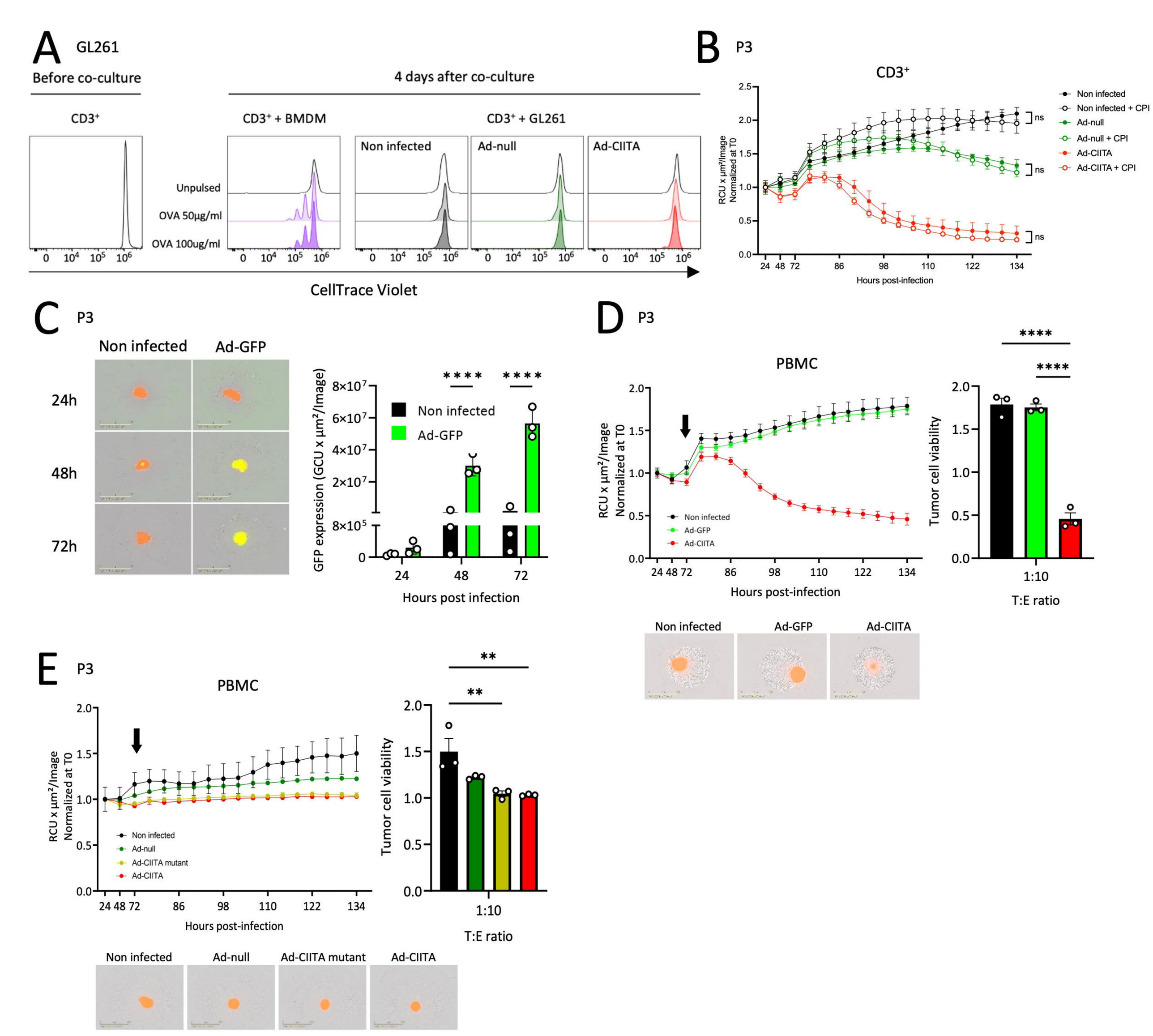
A
GL261
Before co-culture
4 days after co-culture
CD3+
CD3+ + BMDM
CD3+ + GL261
Non infected
Ad-null
Ad-CIITA
Unpulsed
OVA 50µg/ml
OVA 100ug/ml
CellTrace Violet
B
P3
CD3+
RCU x µm²/Image Normalized at T0
Hours post-infection
Non infected
Non infected + CPI
Ad-null
Ad-null + CPI
Ad-CIITA
Ad-CIITA + CPI
ns
C
P3
Non infected
Ad-GFP
24h
48h
72h
GFP expression (GCU x µm²/Image)
Hours post infection
D
P3
PBMC
RCU x µm²/Image Normalized at T0
Hours post-infection
Tumor cell viability
T:E ratio
1:10
Non infected
Ad-GFP
Ad-CIITA
E
P3
PBMC
RCU x µm²/Image Normalized at T0
Hours post-infection
Non infected
Ad-null
Ad-CIITA mutant
Ad-CIITA
Tumor cell viability
T:E ratio
1:10

Figure 5

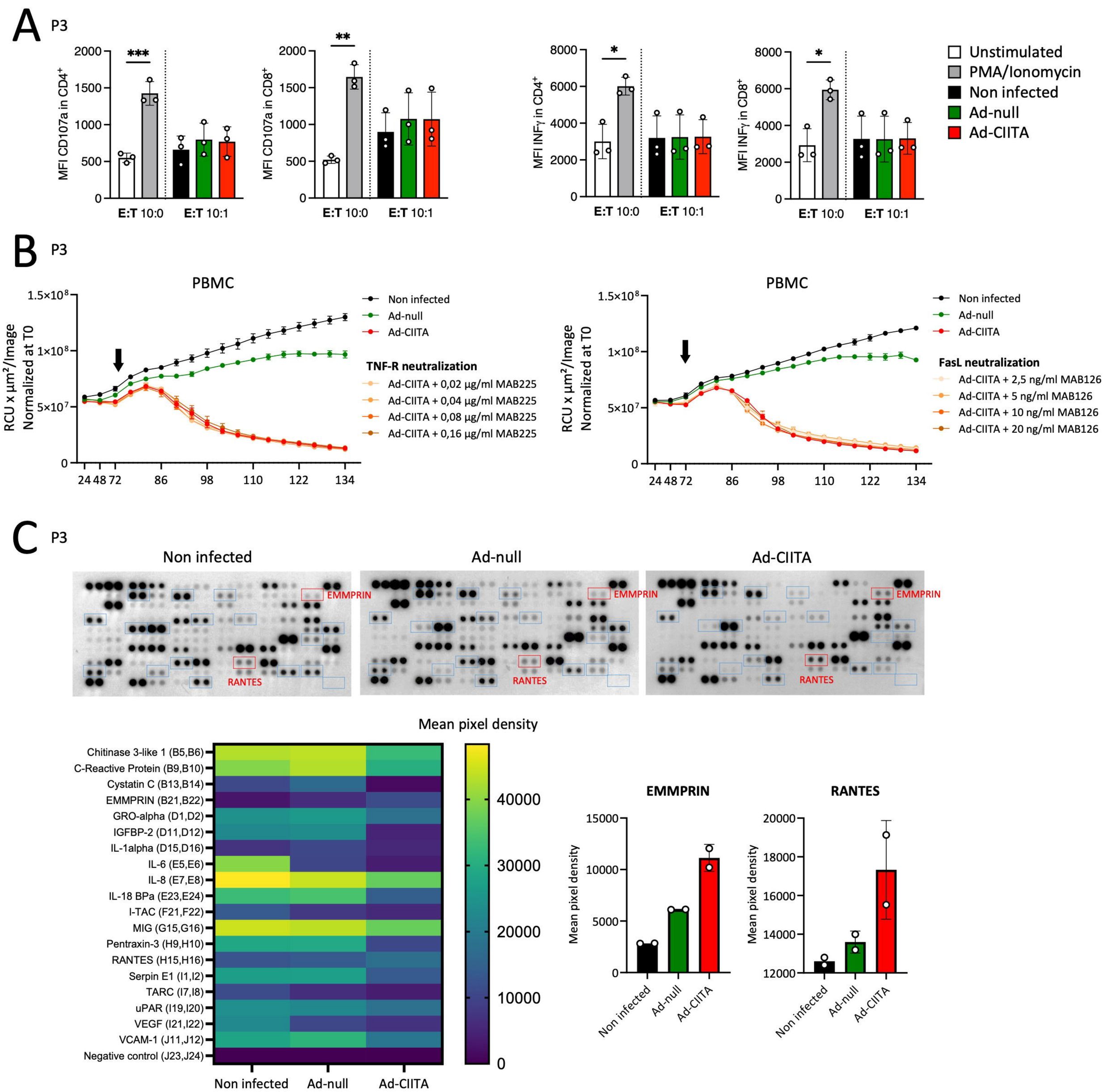
A
P3
MFI CD107a in CD4+
MFI CD107a in CD8+
MFI INFγ in CD4+
MFI INFγ in CD8+
E:T 10:0
E:T 10:1
Unstimulated
PMA/Ionomycin
Non infected
Ad-null
Ad-CIITA
B
P3
PBMC
RCU x µm²/Image Normalized at T0
Non infected
Ad-null
Ad-CIITA
TNF-R neutralization
Ad-CIITA + 0,02 µg/ml MAB225
Ad-CIITA + 0,04 µg/ml MAB225
Ad-CIITA + 0,08 µg/ml MAB225
Ad-CIITA + 0,16 µg/ml MAB225
FasL neutralization
Ad-CIITA + 2,5 ng/ml MAB126
Ad-CIITA + 5 ng/ml MAB126
Ad-CIITA + 10 ng/ml MAB126
Ad-CIITA + 20 ng/ml MAB126
C
P3
Non infected
Ad-null
Ad-CIITA
EMMPRIN
RANTES
Mean pixel density
Chitinase 3-like 1 (B5,B6)
C-Reactive Protein (B9,B10)
Cystatin C (B13,B14)
EMMPRIN (B21,B22)
GRO-alpha (D1,D2)
IGFBP-2 (D11,D12)
IL-1alpha (D15,D16)
IL-6 (E5,E6)
IL-8 (E7,E8)
IL-18 BPa (E23,E24)
I-TAC (F21,F22)
MIG (G15,G16)
Pentraxin-3 (H9,H10)
RANTES (H15,H16)
Serpin E1 (I1,I2)
TARC (I7,I8)
uPAR (I19,I20)
VEGF (I21,I22)
VCAM-1 (J11,J12)
Negative control (J23,J24)
Mean pixel density

Figure 6

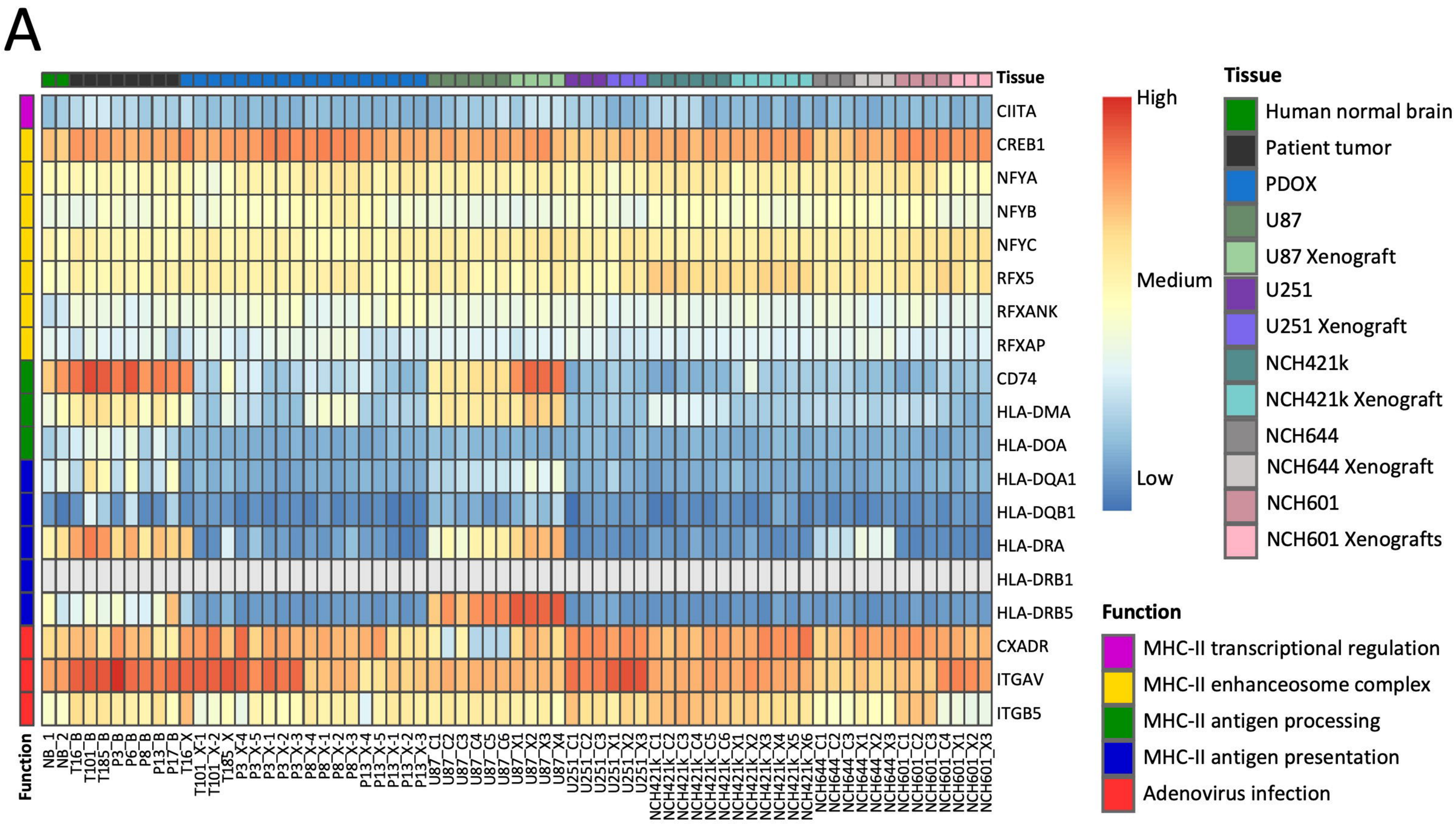

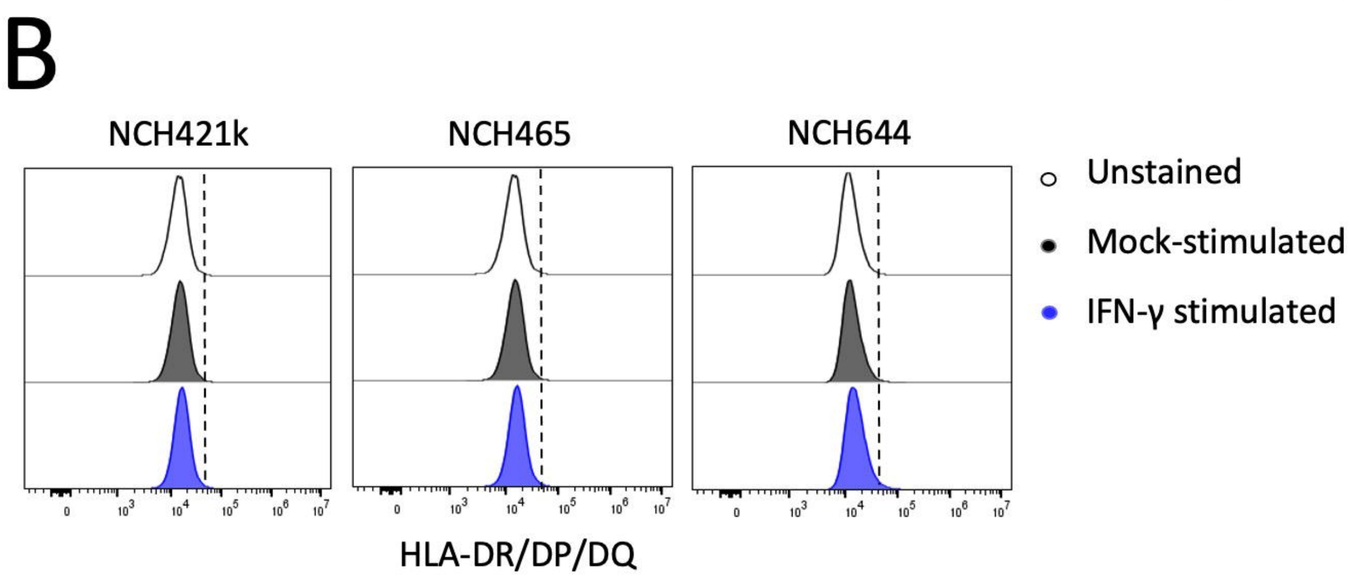

Supplementary Figure 1

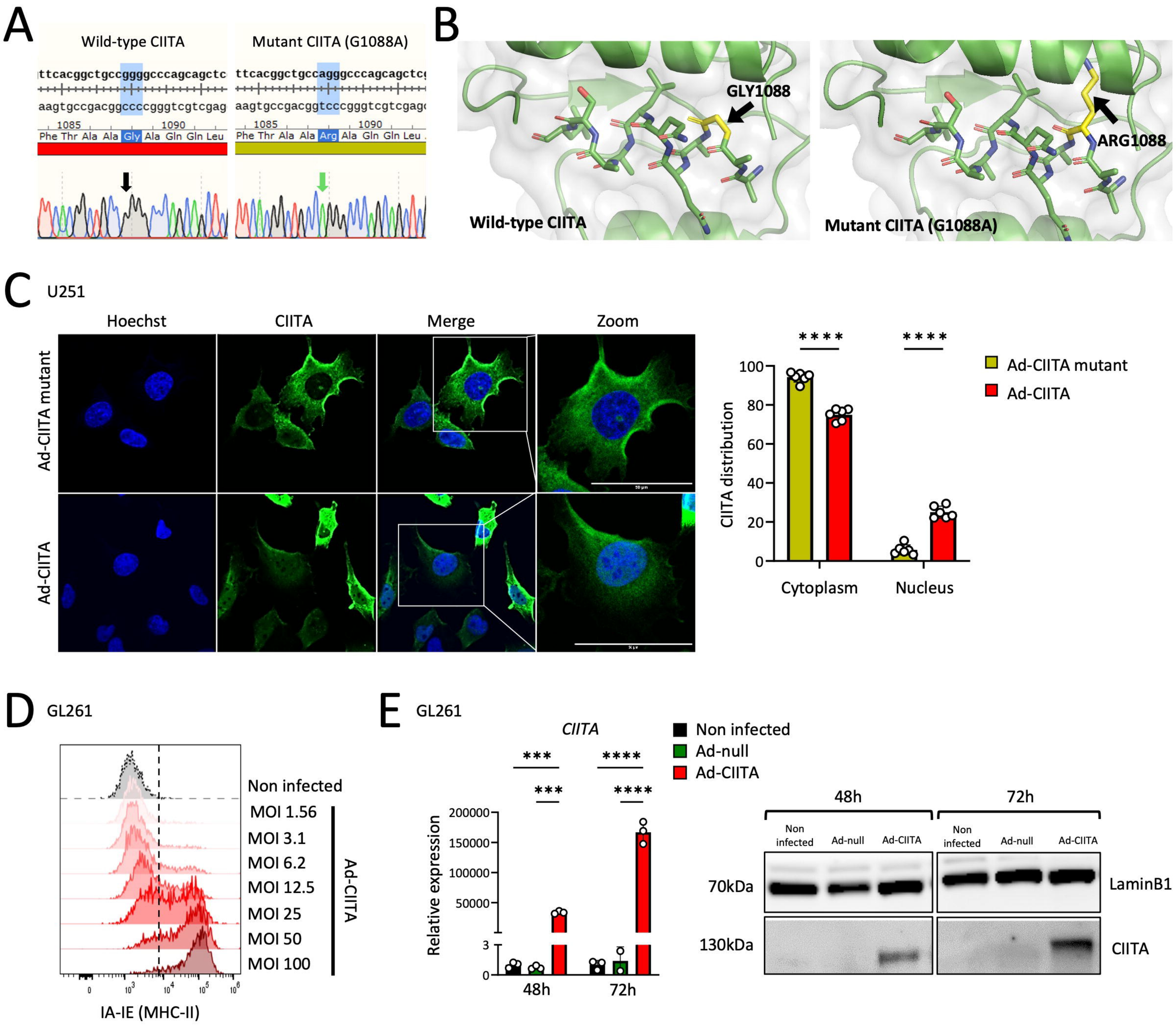

Supplementary Figure 2

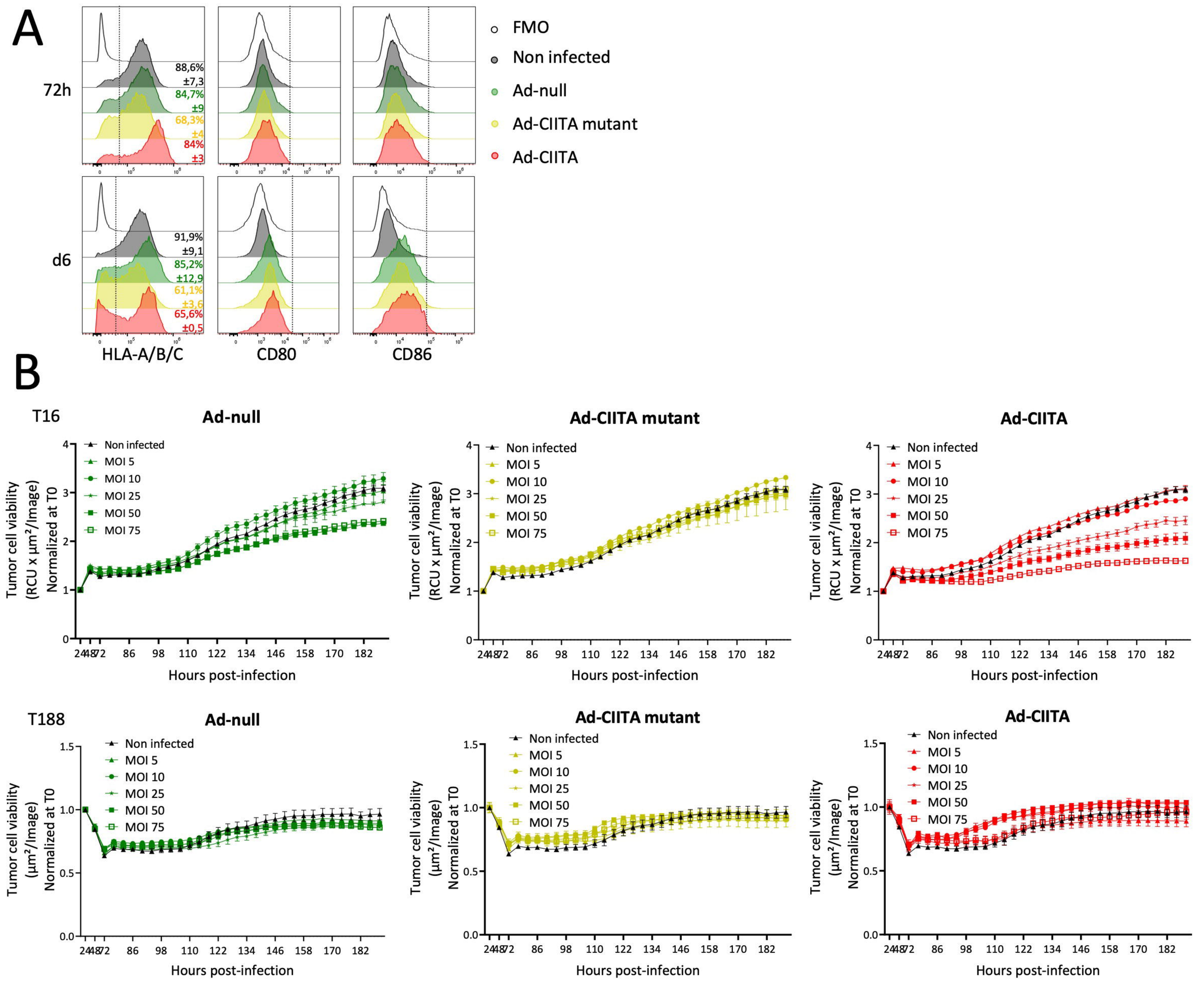

Supplementary Figure 3

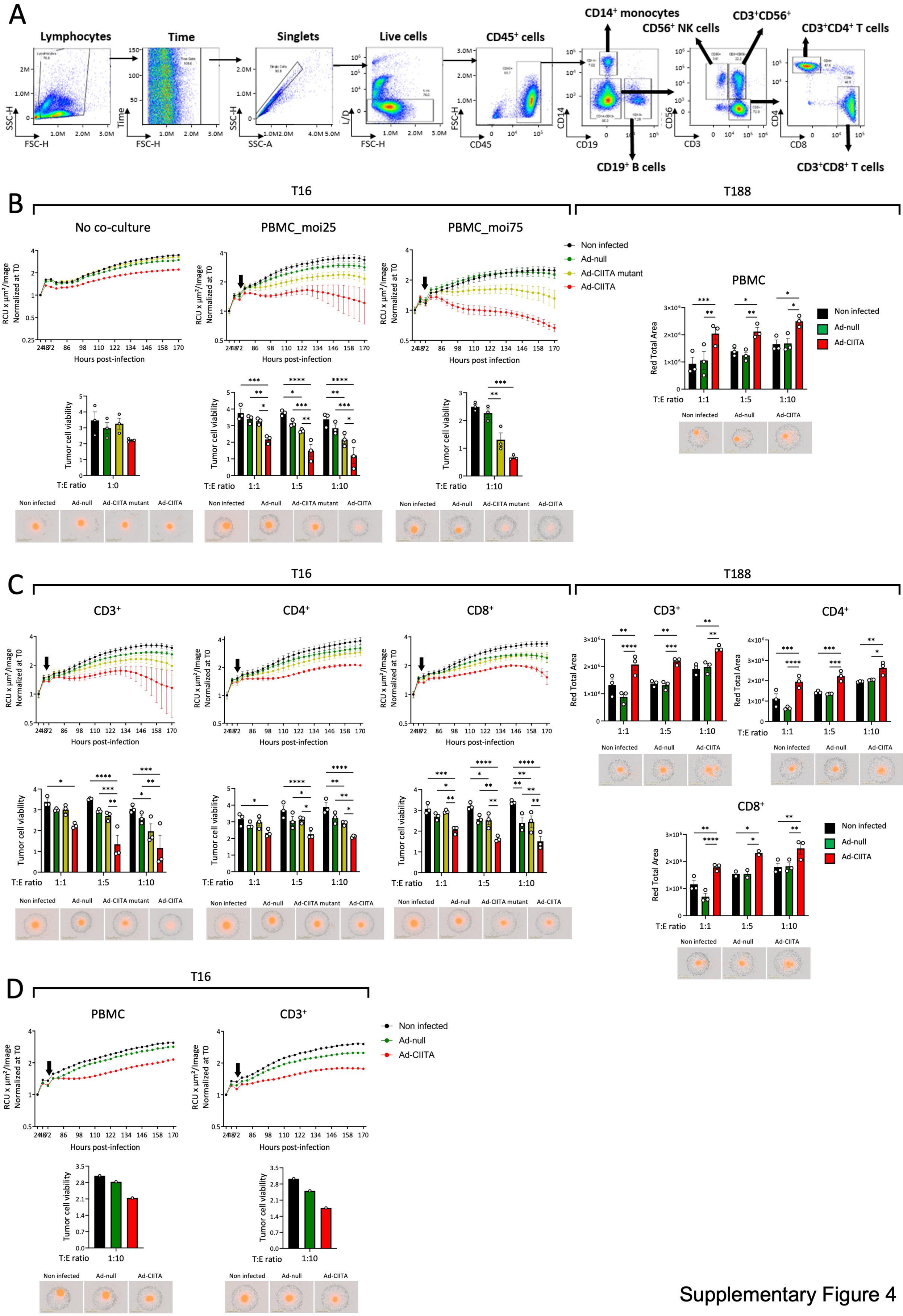

Supplementary Figure 4

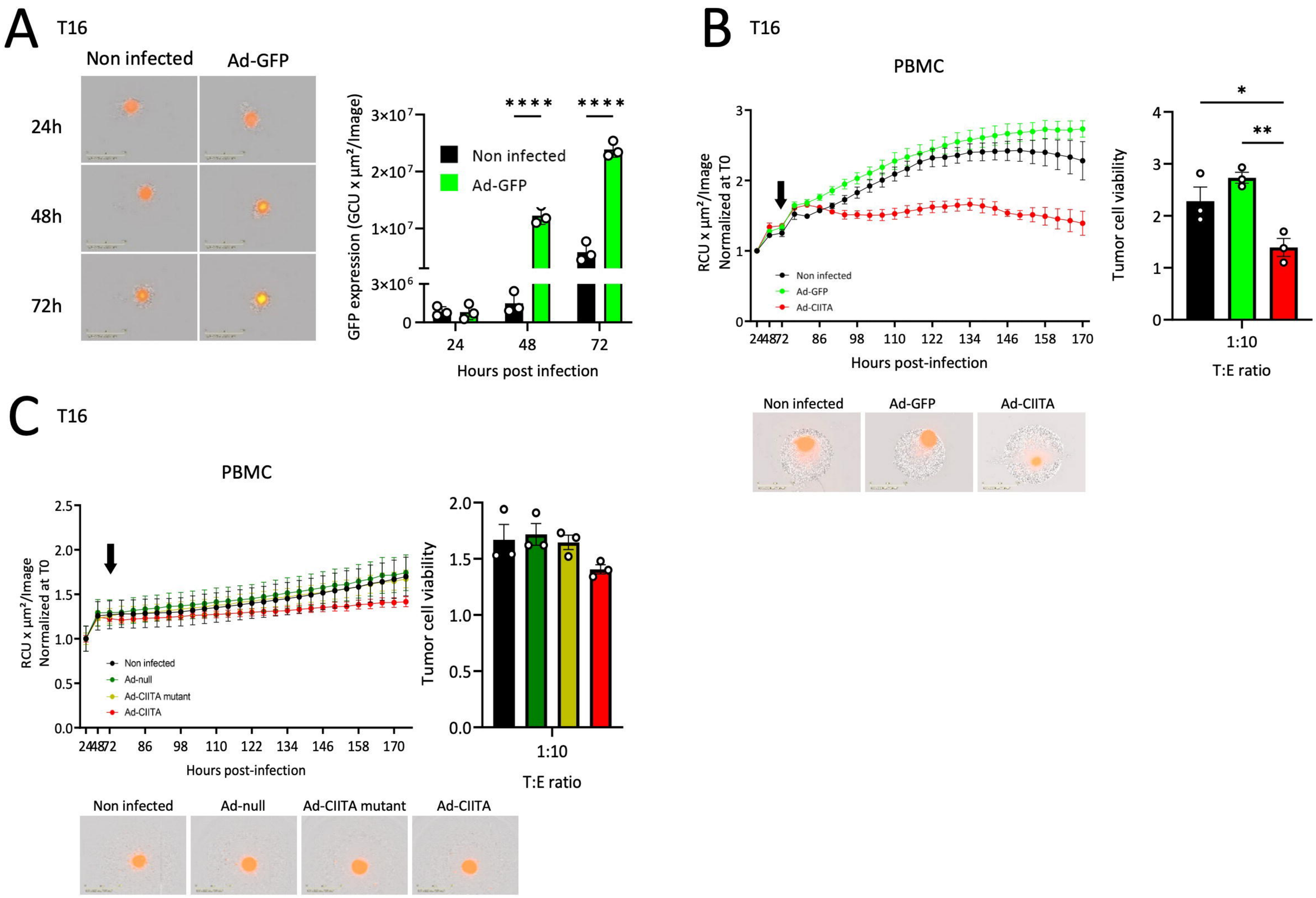

Supplementary Figure 5

P3

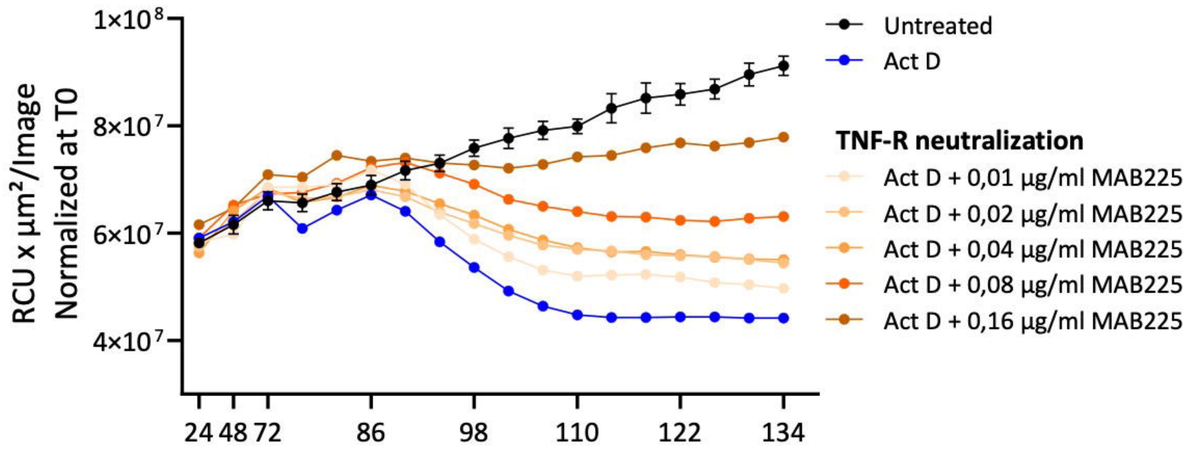

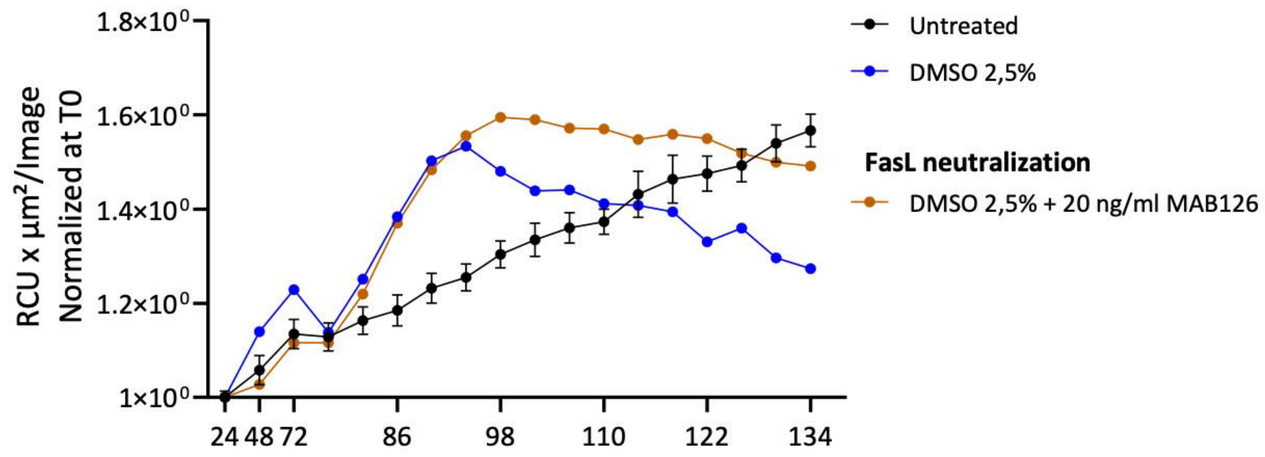

Supplementary Figure 6